VIROLOGY

Targeting highly pathogenic coronavirus-induced apoptosis reduces viral pathogenesis and disease severity

Hin Chu[1,2,3†], Huiping Shuai[1,2†], Yuxin Hou[2], Xi Zhang[2], Lei Wen[2], Xiner Huang[2], Bingjie Hu[2], Dong Yang[2], Yixin Wang[2], Chaemin Yoon[2], Bosco Ho-Yin Wong[2], Cun Li[2], Xiaoyu Zhao[2], Vincent Kwok-Man Poon[2], Jian-Piao Cai[2], Kenneth Kak-Yuen Wong[4], Man-Lung Yeung[1,2,3], Jie Zhou[1,2,3], Rex Kwok-Him Au-Yeung[5], Shuofeng Yuan[1,2,3], Dong-Yan Jin[6], Kin-Hang Kok[1,2], Stanley Perlman[7], Jasper Fuk-Woo Chan[1,2,3,8,9*], Kwok-Yung Yuen[1,2,3,8,9*]

Infection by highly pathogenic coronaviruses results in substantial apoptosis. However, the physiological relevance of apoptosis in the pathogenesis of coronavirus infections is unknown. Here, with a combination of in vitro, ex vivo, and in vivo models, we demonstrated that protein kinase R–like endoplasmic reticulum kinase (PERK) signaling mediated the proapoptotic signals in Middle East respiratory syndrome coronavirus (MERS-CoV) infection, which converged in the intrinsic apoptosis pathway. Inhibiting PERK signaling or intrinsic apoptosis both alleviated MERS pathogenesis in vivo. Severe acute respiratory syndrome coronavirus 2 (SARS-CoV-2) and SARS-CoV induced apoptosis through distinct mechanisms but inhibition of intrinsic apoptosis similarly limited SARS-CoV-2– and SARS-CoV–induced apoptosis in vitro and markedly ameliorated the lung damage of SARS-CoV-2–inoculated human angiotensin-converting enzyme 2 (hACE2) mice. Collectively, our study provides the first evidence that virus-induced apoptosis is an important disease determinant of highly pathogenic coronaviruses and demonstrates that this process can be targeted to attenuate disease severity.

INTRODUCTION

Three highly pathogenic coronaviruses have emerged over the past two decades and resulted in substantial mortality and morbidity. Severe acute respiratory syndrome coronavirus (SARS-CoV) emerged in 2002 and resulted in 8096 cases and 774 deaths in less than a year (*1*). Middle East respiratory syndrome coronavirus (MERS-CoV) was identified in 2012 and has resulted in 2564 cases with 881 deaths as of December 2020 (*2*). Recently, SARS-CoV-2 emerged in December 2019 and has quickly spread among the human population, resulting in more than 100 million cases and more than 2 million deaths in approximately a year (*3*, *4*). Infection by these highly pathogenic coronaviruses primarily results in respiratory symptoms including cough and shortness of breath and could develop into severe pneumonia with associated acute respiratory distress syndrome (ARDS). Despite the impact of these highly pathogenic coronaviruses, current research has been focused on their prevention and antiviral treatment. The underlying mechanism accounting for the high pathogenicity of these human pathogenic coronaviruses remains poorly understood.

Apoptosis is a highly regulated form of cell death that can be initiated by the host to limit virus propagation (*5*). However, excessive apoptosis disrupts the architecture and integrity of the bronchoalveolar network and contributes to lung injury and ARDS (*6*). Current knowledge on coronavirus-induced apoptosis is limited. SARS-CoV–induced apoptosis was described in multiple tissues in infected patients (*7*, *8*), and diverse SARS-CoV components were shown to trigger apoptosis (*9*–*11*). We and others demonstrated that MERS-CoV triggered apoptosis in human lung epithelial cells (*12*), human primary T cells (*13*), and lung and kidney cells of MERS-CoV–infected marmosets (*14*). Recently, SARS-CoV-2–induced apoptosis was detected in infected primary human tracheobronchial epithelial cells (*15*), human alveolar organoids (*16*), lungs of SARS-CoV–infected hamsters (*17*), and lung biopsy specimens of patients with Coronavirus Disease 2019 (COVID-19) (*18*). In contrast to SARS-CoV, the mechanism of SARS-CoV-2– and MERS-CoV–induced apoptosis remains largely unexplored. Despite the frequent detection of apoptosis during SARS-CoV-2, SARS-CoV, and MERS-CoV infections, the role of apoptosis in the pathogenesis of these highly pathogenic coronaviruses is unknown.

In the present study, by using MERS-CoV as a model of the highly pathogenic coronaviruses, we investigated the physiological relevance of apoptosis in the pathogenesis of MERS-CoV with a combination of in vitro, ex vivo, and in vivo models. We identified protein kinase R–like endoplasmic reticulum kinase (PERK) signaling as a key modulator of MERS-CoV–triggered apoptosis. We further demonstrated that the proapoptotic signals downstream of PERK signaling converged at the intrinsic apoptosis pathway and that inhibition of PERK signaling or intrinsic apoptosis both significantly alleviated the pathogenesis of MERS-CoV in vivo. Inhibition of intrinsic apoptosis similarly limited SARS-CoV-2– and SARS-CoV–induced

[1]State Key Laboratory of Emerging Infectious Diseases, Li Ka Shing Faculty of Medicine, The University of Hong Kong, Pokfulam, Hong Kong Special Administrative Region, China. [2]Department of Microbiology, Li Ka Shing Faculty of Medicine, The University of Hong Kong, Pokfulam, Hong Kong Special Administrative Region, China. [3]Carol Yu Centre for Infection, Li Ka Shing Faculty of Medicine, The University of Hong Kong, Pokfulam, Hong Kong Special Administrative Region, China. [4]Department of Surgery, Li Ka Shing Faculty of Medicine, The University of Hong Kong, Pokfulam, Hong Kong Special Administrative Region, China. [5]Department of Pathology, Li Ka Shing Faculty of Medicine, The University of Hong Kong, Pokfulam, Hong Kong Special Administrative Region, China. [6]School of Biomedical Sciences, Li Ka Shing Faculty of Medicine, The University of Hong Kong, Pokfulam, Hong Kong Special Administrative Region, China. [7]Department of Microbiology and Immunology, University of Iowa, Iowa City, IA 52242, USA. [8]Department of Clinical Microbiology and Infection Control, The University of Hong Kong–Shenzhen Hospital, Shenzhen, Guangdong Province, China. [9]Hainan Medical University–The University of Hong Kong Joint Laboratory of Tropical Infectious Diseases, The University of Hong Kong, Pokfulam, Hong Kong Special Administrative Region, China.
*Corresponding author. Email: kyyuen@hku.hk (K-Y.Y.) jfwchan@hku.hk (J.F-W.C.)
†These authors contributed equally to this work.

apoptosis in vitro and markedly ameliorated the lung damage of SARS-CoV-2–inoculated human angiotensin-converting enzyme 2 (hACE2) mice. Collectively, our study provides evidence of the critical contribution of apoptosis in human pathogenic coronavirus pathogenesis. Our findings further reveal that apoptosis can be targeted as an effective intervention strategy in the treatment of highly pathogenic coronaviruses including MERS-CoV and SARS-CoV-2.

RESULTS

MERS-CoV infection activates PERK signaling

MERS-CoV induced substantial caspase-dependent apoptosis in ex vivo human lung explants and the lungs of infected human dipeptidyl peptidase 4 (hDPP4) mice, suggesting that apoptosis might play critical physiological roles in MERS-CoV pathogenesis (Fig. 1, A and B). To obtain mechanistic insights into MERS-CoV–induced apoptosis, we interrogated the transcriptomic profile of MERS-CoV–infected human bronchial epithelial Calu3 cells, which contained 1411 and 3821 differentially expressed genes (DEGs) at 12 and 24 hours post-infection (hpi), respectively (*14*). Gene ontology (GO) annotation of the DEGs under the GO term "positive regulation of cell death" identified 73 and 179 potential cell death–associated DEGs at 12 and 24 hpi, respectively (table S1). GO fold enrichment analysis performed using this set of cell death–associated DEGs demonstrated an overrepresentation of genes involved in the endoplasmic reticulum (ER) stress and mitochondrial/intrinsic apoptosis categories (Fig. 1C and table S2). Further analyses of the top cell death–associated DEGs revealed a remarkable enrichment of PERK-regulated genes among these top cell death–associated DEGs (Fig. 1, D and E). This finding was supported by the observation that PERK (also known as EIF2AK3) was up-regulated at both 12 and 24 hpi (Fig. 1E). To further explore the potential involvement of PERK in MERS-CoV–induced cell death, we used the Search Tool for the Retrieval of Interacting Genes/Proteins (STRING) database to create a protein-protein interaction (PPI) network of the cell death–associated DEGs using the most direct neighboring genes of PERK (*19*). In this PPI network, we identified 117 nodes and 618 edges including 45 up-regulated and 72 down-regulated genes, demonstrating a potential regulatory role of PERK on the cell death–associated DEGs upon MERS-CoV infection (Fig. 1F). To confirm the activation of PERK signaling upon MERS-CoV infection, we evaluated the expression of activating transcription factor 4 (ATF4) and C/EBP homologous protein (CHOP), hallmark transcription factors regulated by PERK signaling, in MERS-CoV–infected model cell lines. Our data showed that MERS-CoV infection robustly up-regulated ATF4 and CHOP expression in both Calu3 and Huh7 cells (Fig. 1, G to J). We next examined the expression of representative PERK-regulated factors (*20*) in MERS-CoV–infected primary human small-airway epithelial cells. Our data demonstrated that MERS-CoV infection significantly up-regulated the expression of PERK-regulated transcription factors and downstream apoptosis-associated regulators (Fig. 1K). Collectively, our results suggest that MERS-CoV infection activates PERK signaling, which is potentially involved in MERS-CoV–induced apoptosis.

PERK is a master regulator of MERS-CoV–induced apoptosis

Together with inositol-requiring enzyme 1 alpha (IRE1α) and ATF6, PERK is one of the three major sensors of unfolded protein response (UPR), which participates in the regulation of fundamental cell functions including determination of cell fates (*21*). In particular, persistent PERK activation is known to trigger apoptosis (*22*). MERS-CoV–induced apoptosis was significantly ameliorated upon PERK gene depletion (Fig. 2, A and B). In parallel, the PERK inhibitor GSK2656157 significantly reduced apoptosis in MERS-CoV–infected cells in a dose-dependent manner at the nanomolar scale (Fig. 2, C and D). The specific effect of PERK inhibition was further validated with another selective PERK inhibitor, AMG PERK 44, which similarly down-regulated MERS-CoV–induced apoptosis (Fig. 2E). As controls, IRE1α inhibition did not reduce MERS-CoV–induced apoptosis, suggesting that the PERK but not the IRE1α pathway was specifically responsible for mediating apoptosis in MERS-CoV–infected cells (Fig. 2F). Activation of the PERK pathway governs a repertoire of prodeath signals that ultimately converge on the intrinsic apoptosis pathway (*21*, *23*). To further dissect the mechanism of PERK-mediated apoptosis upon MERS-CoV infection, we evaluated the expression of PERK-regulated prodeath signals in infected cells with or without PERK inhibitors. As demonstrated in Fig. 2G, MERS-CoV infection significantly up-regulated a cluster of prointrinsic apoptotic signals regulated by the PERK pathway, including BIM, ERO1α (endoplasmic reticulum oxidoreductase 1 alpha), NOXA, and PUMA (p53 upregulated modulator of apoptosis). Suppressing PERK signaling with selective PERK inhibitors significantly reduced the expression of these prointrinsic apoptotic factors (Fig. 2G). BIM, NOXA, and PUMA are proapoptotic members of the B-cell lymphoma 2 (BCL-2) family (*24*). To further evaluate their involvement in MERS-CoV–induced apoptosis, we treated Huh7 cells with small interfering RNA (siRNA) targeting these genes followed by MERS-CoV infection and assessed apoptosis activation at 48 hpi. Our results demonstrated that siRNA targeting BIM, NOXA, and PUMA significantly reduced MERS-CoV–induced apoptosis (fig. S1), which indicated that these proapoptotic members of the BCL-2 family contributed to MERS-CoV–induced apoptosis. In line with these findings, inhibition of caspase-9, the initiator caspase of intrinsic apoptosis, but not caspase-8, the initiator caspase of extrinsic apoptosis, significantly rescued the viability of MERS-CoV–infected cells (Fig. 2H). Together, our data demonstrate an essential role of PERK signaling in mediating MERS-CoV–induced apoptosis, predominantly through engaging intrinsic apoptotic signals. Apoptosis is recognized as part of the host innate defense, which eliminates infected cells for the overall benefits of the host. Nevertheless, many viruses have evolved strategies that exploit the apoptosis machinery to facilitate their replication (*25*, *26*). To evaluate whether apoptosis plays a role in MERS-CoV replication, we monitored virus replication upon inhibition of PERK-mediated apoptosis. Our data showed that PERK inhibitors and genetic depletion similarly decreased MERS-CoV replication (fig. S2, A to C). We next directly targeted the apoptosis cascade and quantified virus replication. Our data showed that the apoptosis inhibitor z-VAD-fmk suppressed MERS-CoV replication, while the apoptosis inducer etoposide enhanced virus replication (fig. S2, D to F). The PERK and caspase inhibitors did not reduce MERS-CoV-spike (S) pseudovirus entry, suggesting that the observed reduction in virus replication was not due to differences in virus entry (fig. S3). Collectively, these results demonstrate that virus-induced apoptosis mediated by PERK can augment MERS-CoV replication.

Inhibiting PERK signaling markedly reduces apoptosis in MERS-CoV–infected human lung tissues

Next, to investigate the physiological relevance of PERK-mediated apoptosis upon MERS-CoV infection, we recapitulated MERS-CoV

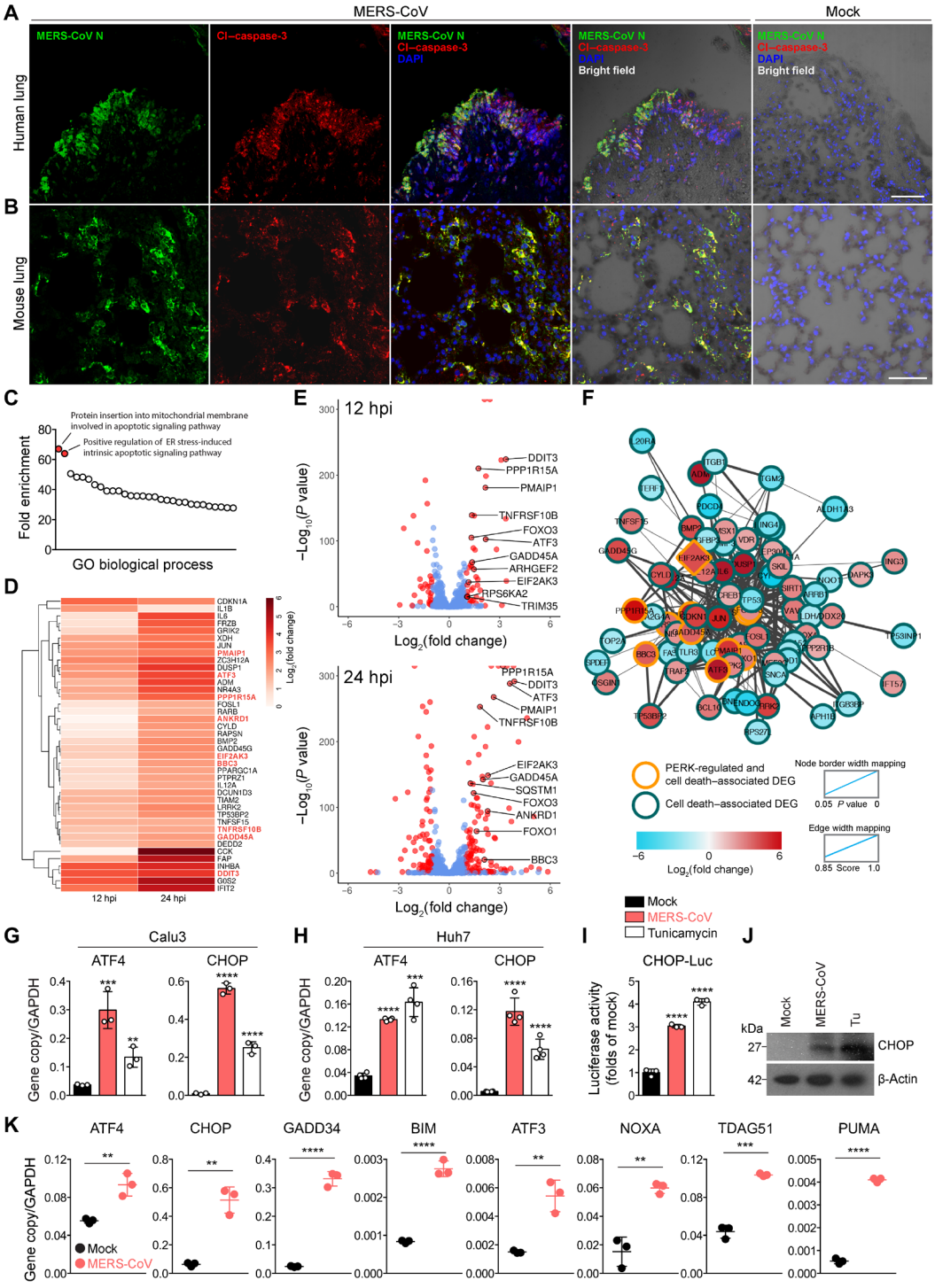

Fig. 1. MERS-CoV infection activates PERK signaling. (**A**) MERS-CoV–infected human lung tissues and (**B**) lungs of MERS-CoV–inoculated hDPP4 mice were immunolabeled for MERS-CoV N, cleaved caspase-3, and 4′,6-diamidino-2-phenylindole (DAPI). Cl-caspase-3, cleaved-caspase-3. (**C**) GO fold enrichment analysis of the cell death–associated DEGs showing the top 30 enriched biological processes with $P < 0.05$ with Bonferroni correction. (**D**) Heatmap demonstrating the top 40 up-regulated cell death–associated DEGs. PERK-regulated genes were highlighted. (**E**) Volcano plots of the cell death–associated DEGs, which were highlighted in red. PERK-regulated genes were labeled. (**F**) STRING-based PPI network of cell death–associated DEGs. The node border width represented *P* value. Cell death–associated DEGs were labeled with green borders, and PERK-regulated cell death–associated DEGs were labeled with orange borders. (**G** and **H**) MERS-CoV–infected Calu3 and Huh7 cells were harvested at 24 hpi for RT-qPCR analysis ($n = 3$ to 4). GAPDH, glyceraldehyde-3-phosphate dehydrogenase. (**I**) CHOP-Luc reporter activity in MERS-CoV–infected Huh7 cells ($n = 3$). (**J**) CHOP expression in MERS-CoV–infected Huh7 cells. (**K**) Expression of representative PERK-regulated genes in MERS-CoV–infected primary human small-airway epithelial cells ($n = 3$). Data represented means ± SD from the indicated number of biological repeats. Statistical differences were determined with one-way analysis of variance (ANOVA) in (G) to (I) and Student's *t* test in (K). $^{**}P < 0.01$; $^{***}P < 0.001$; $^{****}P < 0.0001$. Scale bars, 50 μm (A and B).

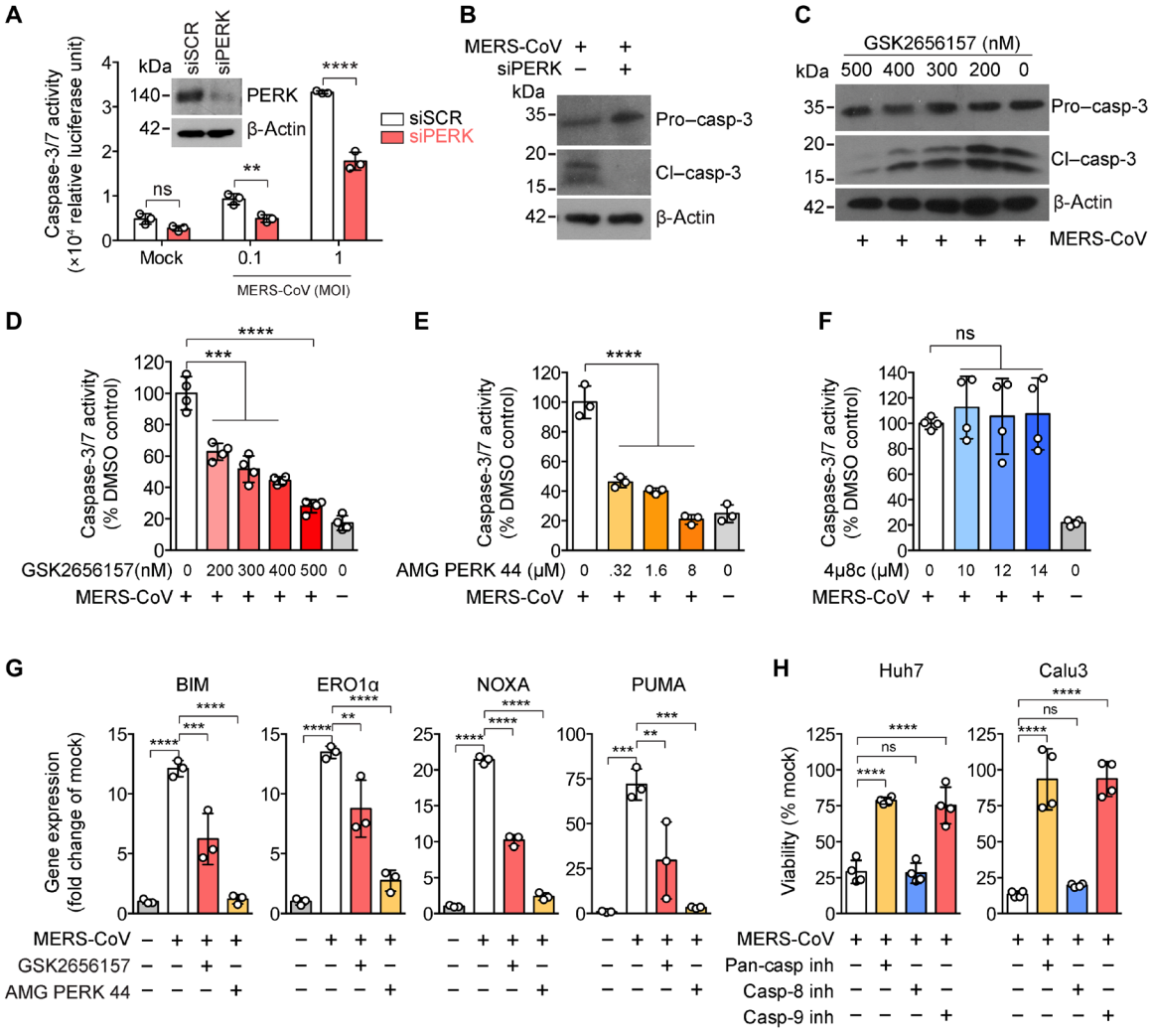

Fig. 2. PERK is a master regulator of MERS-CoV–induced apoptosis. (**A**) PERK or scrambled small interfering RNA (siRNA)–treated Huh7 cells were infected with MERS-CoV. At 24 hpi, apoptosis induction was quantified with caspase-3/7 activity assays ($n = 3$). MOI, multiplicity of infection. (**B**) PERK or scrambled siRNA-treated Huh7 cells were infected with MERS-CoV at 1 MOI. At 24 hpi, caspase-3 cleavage was evaluated with Western blots. (**C**) Western blot detection of caspase-3 cleavage of MERS-CoV–infected Huh7 cells treated with GSK2656157. (**D** to **F**) Huh7 cells were infected with MERS-CoV at 0.01 MOI and treated with GSK2656157 (D), AMG PERK 44 (E), or 4μ8c (F) at the indicated concentrations ($n = 3$ to 4). Apoptosis induction was quantified with caspase-3/7 activity assays at 24 hpi ($n = 3$). DMSO, dimethyl sulfoxide. (**G**) Expression of PERK-regulated prointrinsic apoptotic genes in Huh7 cells upon MERS-CoV infection with GSK2657157 or AMG PERK 44 treatment ($n = 3$). (**H**) MERS-CoV–infected Huh7 and Calu3 cells were treated with DMSO, pan-caspase inhibitor (z-VAD-fmk), caspase-8 inhibitor (z-IETD-fmk), or caspase-9 inhibitor (z-LEHD-fmk). The cell viability at 24 hpi was quantified ($n = 4$). Data represented means ± SD from the indicated number of biological repeats. Statistical difference between groups was determined with one-way ANOVA and was considered significant when $P < 0.05$. $^{**}P < 0.01$; $^{***}P < 0.001$; $^{****}P < 0.0001$. ns, not statistically significant.

infection in ex vivo human lung tissue cultures. In agreement with our in vitro findings, MERS-CoV infection activated PERK signaling in the infected tissues, and inhibition of PERK signaling significantly attenuated the up-regulation of PERK-regulated genes including a subset of prointrinsic apoptotic factors [CHOP, BIM, TRIB3 (tribbles pseudokinase 3), NOXA, and ERO1α] (Fig. 3A). With confocal microscopy, we demonstrated that PERK inhibition with GSK2656157 substantially ameliorated both MERS-CoV–induced apoptosis and virus propagation in the infected human lung tissues (Fig. 3, B and C). The suppression of virus replication by PERK inhibition was further illustrated by immunohistochemistry, quantitative reverse transcription polymerase chain reaction (RT-qPCR), and plaque assays (Fig. 3, D and E) and could similarly be achieved with caspase inhibition (fig. S4). Overall, results from the ex vivo human lung tissues support that PERK signaling mediates MERS-CoV–induced apoptosis, while inhibiting PERK signaling potently suppresses apoptosis and virus growth.

Apoptosis inhibition ameliorates the pathogenesis of human pathogenic coronaviruses in vivo

To dissect whether apoptosis played a role in MERS-CoV pathogenesis in vivo, we investigated the effect of PERK inhibition in hDPP4-transgenic mice upon lethal MERS-CoV challenge (Fig. 4A). We detected the expression of 14 representative PERK-regulated genes in the mice lungs harvested on days 2 and 4 after challenge. Our data showed that 12 of 14 (85.7%) evaluated genes, including a subset of genes that specifically engaged in intrinsic apoptosis, were

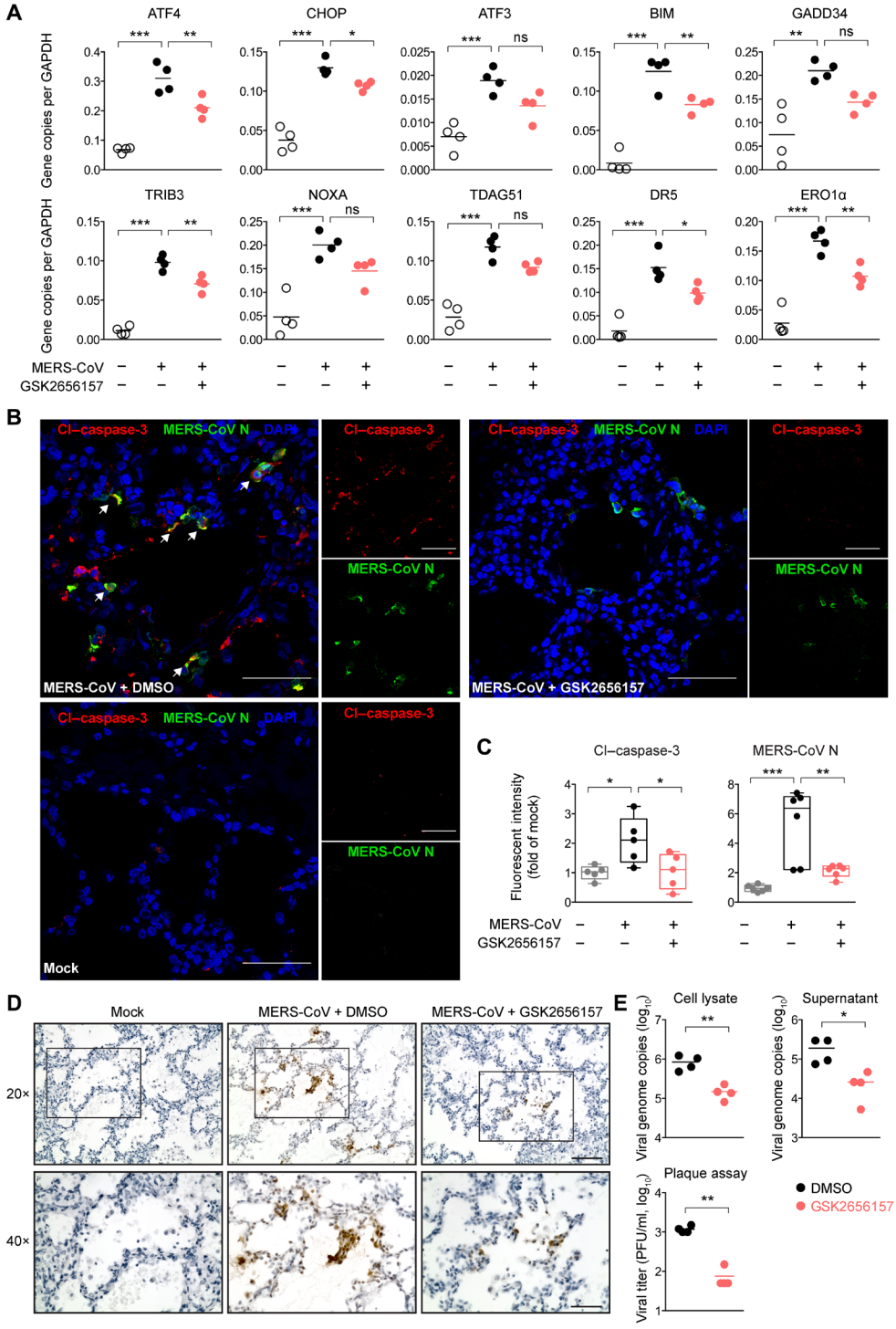

Fig. 3. Inhibiting PERK signaling markedly reduces apoptosis in MERS-CoV–infected human lung tissues. Human lung tissue explants were infected with MERS-CoV with an inoculum of 1×10^8 plaque-forming units (PFU)/ml. The inoculum was removed at 2 hpi and replaced with culture media with or without the PERK inhibitor. Samples were harvested at 24 hpi. (**A**) RT-qPCR analysis of PERK-regulated genes in human lung tissues ($n = 4$). (**B**) Representative immunofluorescence images of MERS-CoV–infected human lung tissues treated with GSK2656157 (top right) or were mock-treated (top left). The images were immunolabeled for cleaved caspase-3 (red) and MERS-CoV N (green). DAPI (blue) was used to identify the cell nuclei. (**C**) Quantitative analyses of caspase-3 activation and MERS-CoV N signals from the infected human lung tissues. Results were presented as boxplots of median ± first to third quartiles with whiskers extended to maxima and minima ($n = 5$ to 6). (**D**) Representative immunohistochemistry images of MERS-CoV–infected human lung tissues. The extent of MERS-CoV infection was identified with MERS-CoV N staining (brown). (**E**) Quantification of virus replication by RT-qPCR and plaque assays ($n = 4$). Results were obtained using human lung tissues from four to six independent donors, as indicated in the respective panels. Statistical difference between groups in (C) and (E) was determined with one-way ANOVA or Student's *t* test, respectively, and was considered significant when $P < 0.05$. *$P < 0.05$; **$P < 0.01$; ***$P < 0.001$. Scale bars, 50 μm (B).

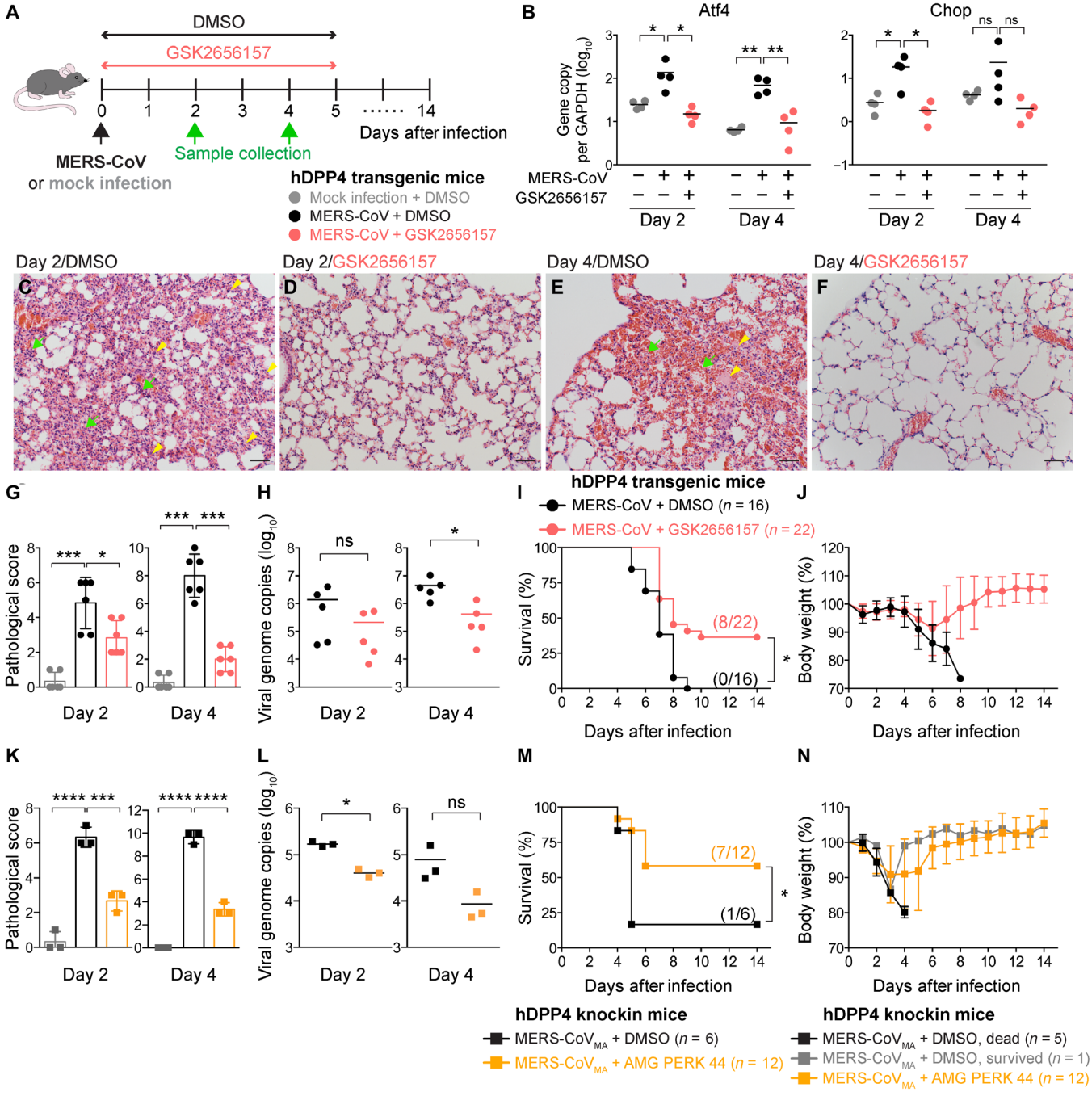

Fig. 4. PERK inhibitors improve the infection outcome of MERS-CoV–inoculated hDPP4 transgenic and KI mice. (**A**) Schematic illustration of the animal experiment. (**B**) Expression of representative PERK-regulated genes was evaluated with RT-qPCR ($n = 4$). (**C** to **F**) Representative images of hematoxylin and eosin (H&E) stain of harvested mouse lungs. (C) Thickened alveolar septa (yellow arrowheads) and severe alveolar septal inflammation by mononuclear cells (green arrows) were detected by day 2 after challenge. (E) Large areas of hemorrhage in the alveolar sacs (green arrows) and fibrin deposition (yellow arrowheads) were detected by day 4 after challenge. (D and F) GSK2656157-treated mice experienced only mild inflammatory infiltration. (**G**) Quantitative analyses of lung pathology ($n = 6$). (**H**) Viral genome copies of the harvested lungs ($n = 5$). (**I** and **J**) Survival and bodyweight of the infected mice. (**K**) Quantitative analyses of lung pathology and (**L**) viral genome copies from MERS-CoV_{MA}–inoculated hDPP4 KI mice ($n = 3$). (**M** and **N**) Survival and bodyweight of MERS-CoV_{MA}–inoculated hDPP4 KI mice treated with AMG PERK 44 or DMSO. Statistical differences were determined with two way-ANOVA in (B), one way-ANOVA in (G) and (K), Student's *t* test in (H) and (L), or log-rank (Mantel-Cox) test in (I) and (M). $^*P < 0.05$; $^{**}P < 0.01$; $^{***}P < 0.001$; $^{****}P < 0.0001$. Scale bars, 50 μm (C to F).

significantly up-regulated after challenge (Fig. 4B and fig. S5A). Expression of 11 (Atf4, Chop, Bim, Noxa, Puma, Gadd34, Sesn2, Chac1, Atf3, Atf5, and Dr5) of the 12 up-regulated genes were significantly attenuated by PERK inhibition on either day 2 or 4 or both after challenge. Severe hemorrhagic pneumonia and diffuse alveolar damage were the predominant histopathological features in severe and fatal MERS cases (*27*). Meanwhile, morphological changes hinted the presence of apoptosis in MERS-CoV–infected human lung tissues that might contribute to lung damage (*28*). Our results in the infected hDPP4-transgenic mice demonstrated that the down-regulation of PERK-regulated apoptotic genes resulted in a marked reduction in the extent of apoptosis as revealed by immunofluorescence staining of caspase-3 activation in mouse lungs (fig. S5, B and C). Furthermore, histological examinations indicated that inhibiting PERK signaling markedly ameliorated MERS-CoV–induced lung damage (Fig. 4, C to F). The dimethyl sulfoxide (DMSO)–treated mice showed marked thickening of the alveolar septa across the lung (yellow arrowheads) with severe infiltration by mononuclear inflammatory cells (green arrows) on day 2 after challenge (Fig. 4, C and G). By day 4 after challenge, extensive hemorrhage (green arrows) in the alveoli and fibrin deposits (yellow arrowheads) were detected in multiple areas of the infected mouse lung (Fig. 4, E and G). However, comparing with their DMSO-treated littermate, GSK2656157-treated mice experienced only mild inflammatory infiltration in the alveolar septa on days 2 and 4 after challenge (Fig. 4, D, F, and G). In addition to these histological findings, inhibiting PERK signaling in vivo significantly suppressed MERS-CoV replication in the lungs of infected mice on day 4 after challenge (Fig. 4H). While all DMSO-treated mice succumbed to MERS-CoV infection, the survival of GSK2656157-treated mice was significantly improved (day 14 survival of DMSO-treated: 0 of 16 or 0% versus GSK2656157-treated: 8 of 22 or 36.4%; $P = 0.0020$) (Fig. 4, I and J). In addition to the hDPP4 transgenic mice, we further evaluated the impact of apoptosis in MERS-CoV pathogenesis in the hDPP4 exon 10 to 12 knockin (KI) mice. In this model, the selective PERK inhibitor AMG PERK 44 significantly reduced lung pathology and viral load (Fig. 4, K and L) and improved the survival of mouse-adapted MERS-CoV (MERS-CoV_{MA})–infected hDPP4 KI mice from 16.7% (1 of 6) to 58.3% (7 of 12) ($P = 0.0350$) (Fig. 4, M and N). Together, our results demonstrate that PERK-regulated apoptosis contributes to MERS-CoV pathogenesis. Intervention with PERK-specific inhibitors significantly ameliorates virus-induced apoptosis, attenuates lung damage, and improves the disease outcome of MERS.

In addition to MERS-CoV, we asked whether apoptosis in SARS-CoV-2 and SARS-CoV infection is also regulated by PERK signaling and could be intervened with PERK inhibitors. SARS-CoV-2 or SARS-CoV M did not disrupt the interaction between 78-kDa glucose-regulated protein (GRP78) and PERK (fig. S6, A and B), and infection by SARS-CoV-2 or SARS-CoV did not activate PERK-regulated markers (fig. S6C). In line with these observations, PERK inhibitors did not suppress SARS-CoV-2– or SARS-CoV–triggered apoptosis (fig. S6D). Because different human pathogenic coronaviruses may trigger apoptosis through diverse upstream mechanisms, which converge in the intrinsic apoptotic pathway, we evaluated whether SARS-CoV-2– or SARS-CoV–induced apoptosis could be inhibited with the intrinsic apoptosis inhibitor z-LEHD-fmk, similar to what we observed in MERS-CoV–induced apoptosis (Fig. 2H). Our results demonstrated that apoptosis induced by both SARS-CoV-2 and SARS-CoV was effectively suppressed by inhibiting intrinsic apoptosis (Fig. 5A). z-LEHD-fmk treatment significantly rescued the survival of MERS-CoV_{MA}–inoculated hDPP4 KI mice from 0% (0 of 9) to 60% (6 of 10) ($P = 0.0035$) (Fig. 5, B and C). Furthermore, by the K18-hACE2 transgenic mouse model, we demonstrated that inhibition of apoptosis with z-LEHD-fmk markedly reduced SARS-CoV-2–induced lung damage, which was evidenced by the reduced hemorrhage and inflammatory cell infiltration in the lung, as well as the alleviated proinflammatory response (Fig. 5, D to F). These findings indicate that although the specific mechanism that governs apoptosis may differ among MERS-CoV, SARS-CoV-2, and SARS-CoV, inhibition of apoptosis consistently ameliorates the pathogenesis of these highly pathogenic coronaviruses.

MERS-CoV membrane protein triggers apoptosis by activating PERK signaling

Next, we sought to identify the MERS-CoV component that activated PERK signaling. We recently demonstrated that ultraviolet-inactivated MERS-CoV remained capable of inducing apoptosis, implying that the structural components of MERS-CoV could mediate apoptosis (*13*). Accordingly, we evaluated the four structural components of MERS-CoV on their capacity to initiate PERK activation. Our results demonstrated that MERS-CoV membrane (M) protein specifically activated PERK signaling as evidenced by the increased expression of ATF4 and CHOP (Fig. 6A). In line with this finding, our result from the caspase-3/7 cleavage assay demonstrated that MERS-CoV M but not S, envelope (E), or N, significantly triggered apoptosis (Fig. 6B), which was further verified by the detection of caspase-3 cleavage with Western blots (Fig. 6C). MERS-CoV M–triggered apoptosis could be consistently detected over time (Fig. 6D) in a dose-dependent manner (Fig. 6E) and can be attenuated with either a pan-caspase inhibitor (Fig. 6F) or a selective PERK inhibitor (Fig. 6G). Thus, our data indicate MERS-CoV M as a major viral determinant of PERK-mediated apoptosis.

MERS-CoV M triggers PERK activation by displacing PERK from GRP78

To further elucidate the mechanism of how MERS-CoV M activates PERK signaling, we evaluated the cellular distribution of MERS-CoV M. Exogenously expressed MERS-CoV M strongly colocalized with the ER marker GRP78. MERS-CoV M appeared to interact and redistribute GRP78 at a perinuclear region (Fig. 7A). In contrast, the redistribution of GRP78 was not detected in vector- or MERS-CoV nucleocapsid (N)–expressing cells (Fig. 7A). MERS-CoV M did not colocalize or disrupt the distribution of another ER marker, protein disulfide isomerase (PDI), suggesting that the interaction between MERS-CoV M and GRP78 was specific (Fig. 7B). Unlike overexpressed M that stays in perinulear compartments, M proteins in coronavirus-infected cells interact with other viral components and traffic toward the cell periphery as virus egress increases (*29*, *30*). In MERS-CoV–infected cells or human lung tissues, GRP78 similarly colocalized with MERS-CoV M and was more readily detected at periphery regions of the infected cells (Fig. 7, C and D). GRP78 is the master regulator of ER stress and governs the UPR. In physiologically healthy cells, PERK is maintained in an inactivated state by binding to GRP78. Under stressed conditions, PERK is dissociated from GRP78, followed by oligomerization, autophosphorylation, and activation (*31*). On the basis of the colocalization between MERS-CoV M and GRP78, we postulated that MERS-CoV M might bind GRP78 and disrupt the interaction between GRP78 and PERK,

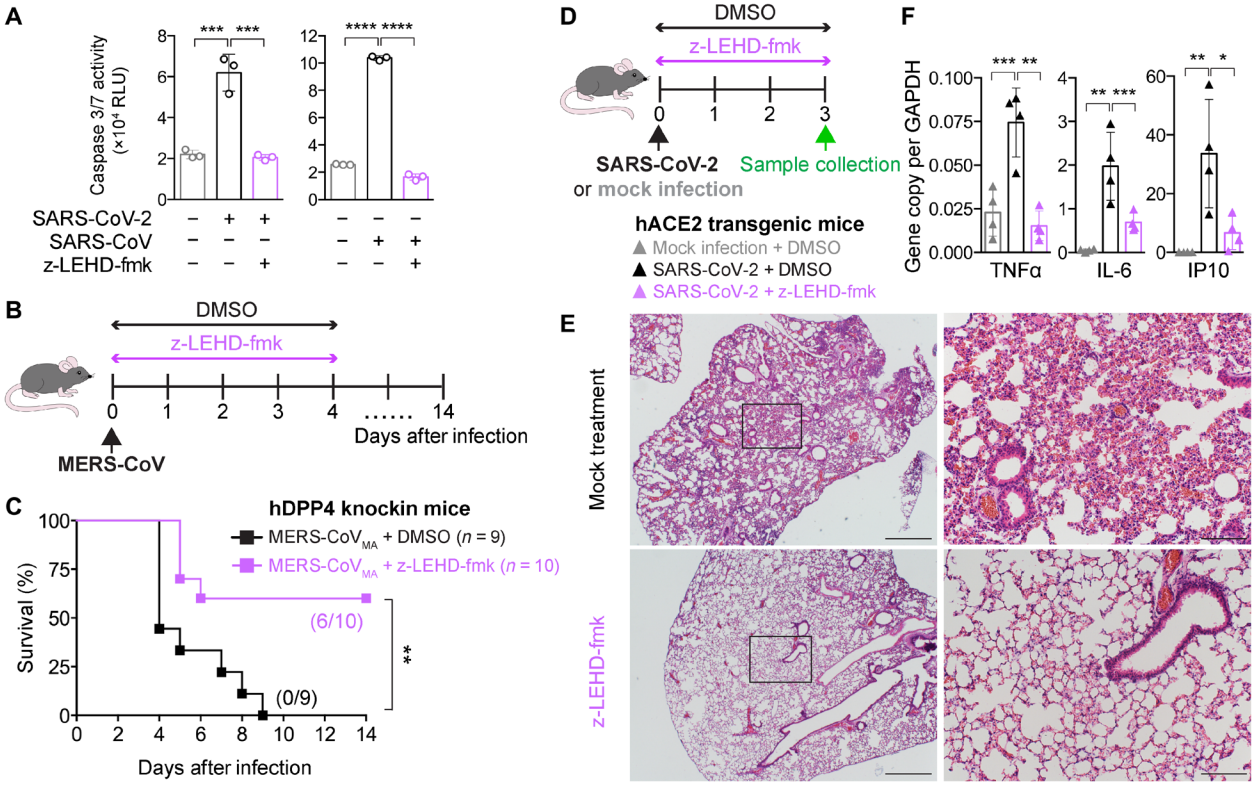

Fig. 5. Inhibition of intrinsic apoptosis improves the infection outcome of the highly pathogenic coronaviruses in vivo. (**A**) SARS-CoV-2– or SARS-CoV–infected Huh7 cells were treated with z-LEHD-fmk or DMSO. Cell lysates were harvested at 24 hpi for caspase-3/7 activity assays ($n = 3$). RLU, relative light unit. (**B**) hDPP4 KI mice were intranasally inoculated with 2500-PFU MERS-CoV$_{MA}$. The mice were intraperitoneally injected with z-LEHD-fmk or DMSO on the indicated days. (**C**) Survival was monitored for 14 days. (**D**) hACE2 transgenic mice were intranasally inoculated with 2.5×10^4-PFU SARS-CoV-2. The mice were intraperitoneally injected with z-LEHD-fmk or DMSO on the indicated days. Lung samples were harvested on day 3 after challenge. (**E**) Lung pathology of SARS-CoV-2–inoculated hACE2 mice with z-LEHD-fmk or DMSO treatment was evaluated with H&E stain. Boxed area was imaged and presented at a higher magnification. (**F**) Expression level of proinflammatory cytokines was determined with qPCR ($n = 4$). Results in (A) and (F) were obtained using three to four biologically independent samples, as indicated in the respective panels. Statistical difference between groups was determined with one way-ANOVA in (A) and (F) or log-rank (Mantel-Cox) test in (C) and was considered significant when $P < 0.05$. *$P < 0.05$; **$P < 0.01$; ***$P < 0.001$; ****$P < 0.0001$. Scale bars, 500 μm (larger view) and 100 μm (inset) (E). TNFα, tumor necrosis factor–α; IL-6, interleukin-6; IP10, interferon gamma-induced protein 10.

resulting in PERK activation. To address this possibility, we first analyzed the interaction between MERS-CoV M and GRP78. Using coimmunoprecipitation, our data showed that MERS-CoV M but not N could physically bind to GRP78 (Fig. 7E). The interaction between GRP78 and PERK was markedly reduced in the presence of MERS-CoV M (Fig. 7F), suggesting that the binding between MERS-CoV M and GRP78 disrupted the association between GRP78 and PERK. Coronavirus M protein is essential for particle formation (*30*, *32*). Mutations in each of the different domains of the protein markedly attenuate virus assembly (*33*, *34*). To dissect the specific domain that was responsible for inducing apoptosis, we constructed M mutants with sequential deletions of the individual transmembrane domain (Fig. 7G). We then overexpressed wild-type M or M mutants and quantified the level of apoptosis induction with Western blots or caspase-3/7 activity assays. Our results indicated that while the M mutant MΔTM1 retained the capacity to induce apoptosis, MΔTM12 or MΔTM123 no longer triggered apoptosis, which suggests that the transmembrane domain 2 of the M protein is responsible for apoptosis induction (Fig. 7, H and I). Overall, our results demonstrate that MERS-CoV M triggers apoptosis by activating PERK signaling through dissociating GRP78 from PERK (fig. S7).

DISCUSSION

Infections by highly pathogenic coronaviruses including SARS-CoV-2, MERS-CoV, and SARS-CoV result in substantial apoptosis in infected cells and tissues. However, the physiological relevance of apoptosis in the pathogenesis of human pathogenic coronaviruses is unknown. Here, by using MERS-CoV as a model, we investigated the mechanism of MERS-CoV–induced apoptosis and determined the physiological relevance of apoptosis in MERS pathogenesis with a combination of in vitro, ex vivo, and in vivo models. We identified PERK signaling as the key regulator of the proapoptotic mediators in MERS-CoV infection, which converged in the intrinsic apoptosis pathway. Inhibition of PERK signaling or intrinsic apoptosis both attenuated MERS pathogenesis in vivo. Inhibition of intrinsic apoptosis similarly suppressed SARS-CoV-2– and SARS-CoV–induced apoptosis in vitro and ameliorated the lung damage in SARS-CoV-2–infected hACE2 mice. Together, our results demonstrate that apoptosis contributes to the pathogenesis of human pathogenic coronaviruses and that this process can be targeted to attenuate disease severity.

Considerable evidence suggests that apoptosis of the alveolar epithelium contributes to lung injury (*6*). During virus infections, while apoptosis serves to eliminate infected cells to limit virus propagation,

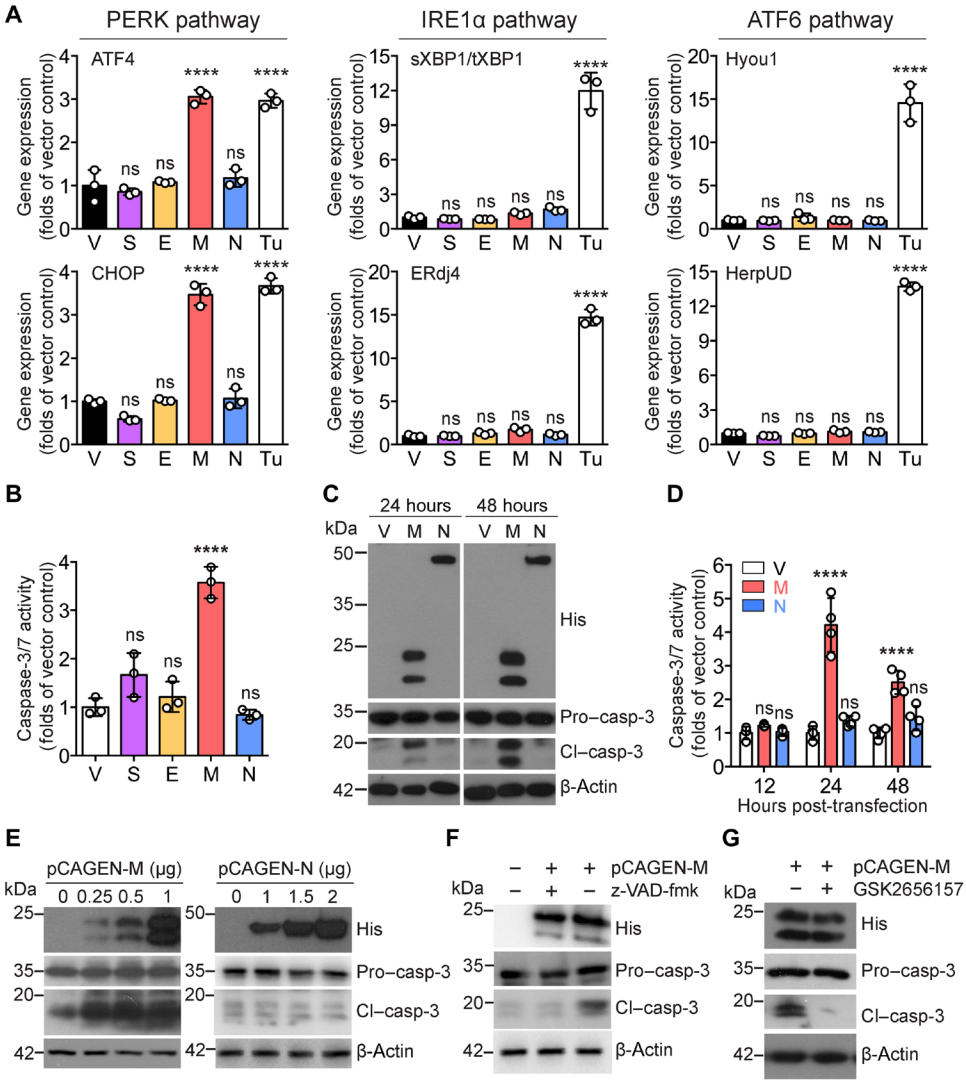

Fig. 6. MERS-CoV M protein triggers apoptosis by activating PERK signaling. (**A**) MERS-CoV S–, E–, M–, or N–expressing Huh7 cells were harvested at 24 hpi. Representative gene expressions for the PERK (ATF4 and CHOP), IRE1α (sXBP1/tXBP1 and ERdj4), and ATF6 (Hyou1 and HerpUD) pathways were determined ($n = 3$). sXBP1/tXBP1 represented the ratio of the spliced form of XBP1 over total XBP1. (**B**) Apoptosis activation by MERS-CoV M expression in Huh7 cells was quantified with caspase-3/7 activity assays ($n = 3$). (**C**) Caspase-3 cleavage in MERS-CoV M–expressing Huh7 cells was detected with Western blots. (**D**) Apoptosis activation by MERS-CoV M expression in Huh7 cells at 12, 24, and 48 hpi was quantified with caspase-3/7 activity assays ($n = 4$). (**E**) Dose-dependent induction of apoptosis by MERS-CoV M was analyzed by Western blot detection of caspase-3 cleavage. (**F** and **G**) MERS-CoV M–transfected Huh7 cells were treated with the pan-apoptosis inhibitor z-VAD-fmk (F) or the PERK inhibitor GSK2656157 (G). Caspase-3 cleavage was detected by Western blots. Data represented means ± SD from the indicated number of biological repeats. Statistical difference between groups was determined with one-way ANOVA and was considered significant when $P < 0.05$. ****$P < 0.0001$.

the exacerbated apoptotic response may impair epithelial integrity, leading to barrier disruption and unfavorable outcomes. In influenza virus infections, virus-induced apoptosis has been thoroughly investigated and is considered predominantly proviral and lung destructive (*35*, *36*). In contrast, despite the fact that apoptosis was documented in SARS-CoV-2, SARS-CoV, and MERS-CoV infections, its physiological role during the infection of human pathogenic coronaviruses has never been addressed. In this regard, our report provides clear evidence that virus-induced apoptosis contributes to lung damage and increases pathogenicity in human pathogenic coronavirus infection.

The precise proapoptotic pathway operative during MERS-CoV infection is largely unknown. Here, we demonstrate that MERS-CoV–induced apoptosis was regulated by PERK signaling, which was previously implicated in apoptosis induced by infectious bronchitis virus, a gammacoronavirus (*37*). MERS-CoV infection resulted in the up-regulated expression of PERK-regulated effectors including CHOP, BIM, NOXA, and PUMA, which are key activators of the intrinsic apoptosis pathway. In line with these findings, an intrinsic apoptosis inhibitor rescued the viability of MERS-CoV–infected cells and MERS-CoV–inoculated hDPP4 KI mice. Together, our data are congruous with the notion that PERK-governed apoptosis during MERS-CoV infection is not mediated through a single signal but is orchestrated through a repertoire of diverse mechanisms that ultimately converge on the intrinsic apoptosis pathway. Apoptosis induced by SARS-CoV-2 and SARS-CoV was similarly attenuated

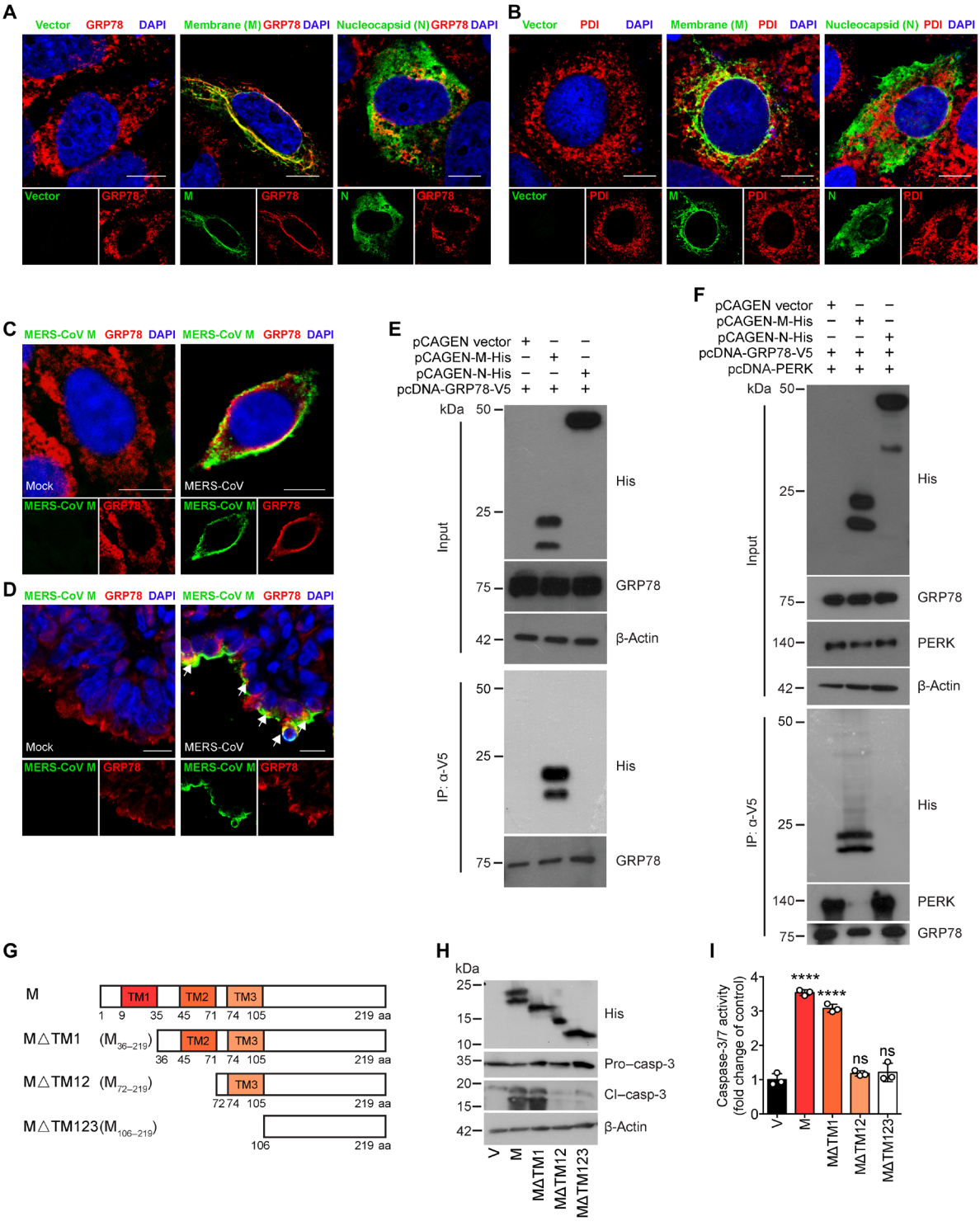

Fig. 7. MERS-CoV M triggers PERK activation by displacing PERK from GRP78. (**A** and **B**) The cellular localization of exogenously expressed MERS-CoV M or N protein and GRP78 was determined with confocal microscopy. (**C** and **D**) The cellular localization of MERS-CoV M and GRP78 in infected Huh7 cell (C) or human lung tissue (D) was determined with confocal microscopy. (**E**) 293 T cells were transfected with MERS-CoV M and GRP78-V5. At 48 hours after transfection, the cells were lysed and immunoprecipitated with an anti-V5 antibody. The presence of coimmunoprecipitated M protein was determined with Western blots. (**F**) 293 T cells were transfected with PERK- and GRP78-expressing plasmids with or without MERS-CoV M. At 48 hours after transfection, the cells were lysed and immunoprecipitated against GRP78-V5. The presence of coimmunoprecipitated PERK was determined with Western blots. (**G**) Schematic of M mutants with sequential transmembrane domain deletions. (**H** and **I**) M and M mutants were expressed in Huh7 cells and were harvested at 48 hours after transfection. Apoptosis induction was evaluated with Western blots (H) or caspase-3/7 activity assays (I) ($n = 3$). Data represented means ± SD from three independent experiments. Statistical difference between groups in (I) was determined with one-way ANOVA and was considered significant when $P < 0.05$. ****$P < 0.0001$. Scale bars, 10 μm (A to D). aa, amino acids.

by the intrinsic apoptosis inhibitor in vitro. At the same time, treatment with the intrinsic apoptosis inhibitor markedly ameliorated the lung damage in SARS-CoV-2–inoculated hACE2 transgenic mice. These findings further indicate that apoptosis inhibition should be investigated as a potential therapeutic strategy in treating the highly pathogenic coronaviruses.

Multiple SARS-CoV components are capable of triggering apoptosis (*9*–*11*). SARS-CoV-2 open reading frame 3a (ORF3a) was recently suggested to induce apoptosis through inducing the release of mitochondrial cytochrome c (*38*). However, the viral component of MERS-CoV that initiates apoptosis remains unknown. Here, our results indicated MERS-CoV M as a key viral determinant of PERK-mediated apoptosis. MERS-CoV M displaced the negative regulator of UPR, GRP78, from binding to PERK, leading to PERK activation. The M protein of coronaviruses is the most abundant structural protein constituting the overall scaffold of the virus and plays an indispensible role during virus assembly (*30*). Stringent requirements must be satisfied for proper M functions during virus assembly, and mutations in any domain of the protein result in attenuated particle formation (*33*). The M proteins of SARS-CoV (*39*) and MERS-CoV (*40*) are also interferon (IFN) antagonists in addition to their roles in virus assembly. Together, MERS-CoV M appears to be a multifaceted viral protein, serving as an essential structural component while modulating virus pathogenesis via inducing apoptosis and inhibiting the IFN response.

The finding that MERS-CoV–induced apoptosis can benefit virus replication is intriguing. Apoptosis is a strategy commonly adopted by the host to eliminate virus-infected cells. To successfully propagate within the host, many viruses have evolved mechanisms to evade apoptosis (*5*, *41*), while other viruses including influenza viruses have developed strategies to exploit the apoptosis machinery for virus replication (*25*, *26*, *42*). We demonstrated here that inhibiting MERS-CoV–induced apoptosis would subsequently diminish virus replication. It is possible that the activated caspase cascade during apoptosis induction may activate certain host pathways that are required for efficient virus replication (*42*). Alternatively, direct caspase cleavage of the viral genome may augment the productive viral life cycle. In both cases, targeting apoptosis may provide dual benefits against MERS-CoV infection.

Our study has a number of limitations. First, the level of apoptosis induction between MERS-CoV, SARS-CoV-2, and SARS-CoV was not evaluated in parallel. Second, the capacity of apoptosis induction by the viral gene products of the three viruses was not compared. Mortality rate differs substantially between the three highly pathogenic coronaviruses including MERS-CoV (~35%), SARS-CoV-2 (~2%), and SARS-CoV (~10%). Knowledge on the relative extent of apoptosis induction between the three viruses and the viral gene products involved may promote our understanding on the pathogenic mechanisms of these human pathogenic coronaviruses. Overall, our study highlights the unfavorable contribution of apoptosis in the pathogenesis of human pathogenic coronaviruses and indicates apoptosis inhibition as a potential therapeutic strategy in the treatment of COVID-19 and MERS.

METHODS

Cell lines and human small-airway epithelial cells

Huh7, 293 T, and VeroE6 cells were maintained in Dulbecco's modified Eagle's medium (DMEM, Gibco) supplemented with 10% heat-inactivated fetal bovine serum (FBS) (Gibco), penicillin (100 U/ml) Gibco), and streptomycin (100 μg/ml) (Gibco). Calu3 cells were cultured in DMEM/F-12 (Gibco) supplemented with 10% FBS, penicillin (100 U/ml), and streptomycin (100 μg/ml). Primary human small-airway epithelial cells were obtained from the American Type Culture Collection (ATCC) and cultured with the airway epithelial cell basal medium supplemented with a bronchial epithelial cell growth kit (ATCC).

Virus

MERS-CoV (GenBank: JX869059.2) was a gift from R. Fouchier (Erasmus Medical Center, Rotterdam, The Netherlands). The MERS-CoV_{MA} was a gift from P. McCray (University of Iowa, IA, USA). SARS-CoV-2 HKU-001a (GenBank accession number MT230904) was isolated from the nasopharyngeal aspirate of a patient with laboratory-confirmed COVID-19 in Hong Kong (*43*). SARS-CoV GZ50 (GenBank accession number AY304495) was an archived clinical isolate at the Department of Microbiology, The University of Hong Kong (HKU). All viruses were propagated and titered in VeroE6 cells with plaque assays as previously described (*43*). All experiments involving infectious MERS-CoV, SARS-CoV-2, and SARS-CoV followed the approved standard operating procedures of our Biosafety Level 3 facility at the Department of Microbiology, HKU.

Ex vivo human lung tissues

Preparation and infection of ex vivo human lung tissues were performed as we previously described (*44*). Briefly, human lung tissues for ex vivo studies were retrieved from patients underwent surgical operations at the Queen Mary Hospital, Hong Kong. All donors gave written consent as approved by the Institutional Review Board of HKU/Hospital Authority Hong Kong West Cluster. Normal non-malignant lung tissue fragments that were in excess for the clinical diagnosis were used. The freshly obtained lung tissues were processed into small rectangular pieces and were rinsed with the primary tissue culture medium, which contained the advanced DMEM/F-12 medium supplemented with 2 mM Hepes (Gibco), 1× GlutaMAX (Gibco), penicillin (100 U/ml), streptomycin (100 μg/ml), vancomycin (20 μg/ml), ciprofloxacin (20 μg/ml), amikacin (50 μg/ml), and nystatin (50 μg/ml). The specimens were infected with MERS-CoV at a titer of 1×10^8 plaque-forming units (PFU)/ml. After 2 hours, the inoculum was removed, and the specimens were washed thoroughly with the primary tissue culture medium. The infected specimens were then transferred to inserts of 12-well Transwells (Corning) precoated with 60% Matrigel (Corning) diluted with the primary tissue culture medium. Subsequently, additional Matrigel mixture was added to the insert to seal the explant. The basolateral compartment was filled with primary tissue culture medium supplemented with 2.5 μM GSK2656157 dissolved in DMSO or DMSO only. The lung tissues were harvested at 24 hpi with either 10% neutral-buffered formalin for immunofluorescence staining or with RL lysis buffer for RT-qPCR analysis.

hDPP4 and ACE2 mouse models

The use of animals was approved by the Committee on the Use of Live Animals in Teaching and Research of HKU. The in-house developed hDPP4 transgenic mice were previously described (*45*). The hDPP4 transgenic mice was inoculated with 40-PFU MERS-CoV prediluted in 20 μl of phosphate-buffered saline (PBS) by intranasal injection, followed by intraperitoneal injection with GSK2656157

(25 mg/kg per day) (Merck) for 6 days or until sample harvest. The hDPP4 exon 10 to 12 KI mice were provided by P. McCray (University of Iowa, IA, USA) and were previously described (*46*). Littermates of the same sex were randomly assigned to experimental groups. On the day of infection, the mice were intranasally inoculated with 2500-PFU MERS-CoV$_{MA}$. Infected mice were treated with AMG PERK44 (25 mg/kg per day) (Tocris) or z-LEHD-fmk (12.5 mg/kg per day) (SelleckChem) for 5 days. For SARS-CoV-2 infection, heterozygous K18-hACE2 transgenic mice, 2B6.Cg-Tg (K18-ACE2) 2Prlmn/J, were obtained from the Jackson laboratory and was previously described (*47*). Littermates of the same sex were randomly assigned to experimental groups. Mice were intranasally inoculated with 2.5×10^4–PFU SARS-CoV-2 and were intraperitoneally treated with z-LEHD-fmk (12.5 mg/kg per day) until sample harvest on day 3 after virus challenge. The health status and weight of the mice were monitored for 14 days on a daily basis or until the animal is sacrificed or euthanized because of reaching the humane end point of the experiment. Mice were euthanized at designated time points, and lung tissue from both treatment and control group mice were harvested for immunofluorescence staining, histopathology examination, or RT-qPCR analysis.

Antibodies

MERS-CoV N was detected with the in-house guinea pig anti–MERS-CoV N serum. MERS-CoV S was detected with the in-house mouse anti–MERS-CoV S immune serum. MERS-CoV M and SARS-CoV-2 M were detected with in-house mouse anti–MERS-CoV M and mouse anti–SARS-CoV-2 M immune serum, respectively. SARS-CoV M was detected with a rabbit anti–SARS-CoV M antibody from Rockland. Primary antibodies including rabbit anti–caspase-3, rabbit anti-PERK, rabbit anti-GRP78, and mouse anti-His were from Abcam. The mouse anti-CHOP antibody was from Cell Signaling Technology. The mouse anti-GRP78 was from R&D Systems. The mouse anti–β-actin was from Sigma-Aldrich. The V5-tagged proteins were detected with a mouse anti-V5 antibody from Immunoway. Secondary antibodies including Alexa Fluor 488 goat anti–guinea pig, Alexa Fluor 488 goat anti-mouse, and Alexa Fluor 568 donkey anti-rabbit were from Thermo Fisher Scientific. The goat anti-mouse horseradish peroxidase (HRP), goat anti-rabbit HRP, and goat anti–guinea pig antibodies from Thermo Fisher Scientific were used for Western blots and immunohistochemistry staining.

PERK, apoptosis, and other chemical modulators

Selective PERK inhibitors GSK2656157 and GSK2606414 were obtained from MedChemExpress, and AMG PERK 44 was obtained from Tocris Bioscience. The IRE1α inhibitor 4μ8c was obtained from Sigma-Aldrich. The pan-caspase inhibitor z-VAD-fmk was obtained from Invivogen. The caspase-8 inhibitor z-IETD-fmk and the caspase-9 inhibitor z-LEHD-fmk were purchased from R&D Systems. The apoptosis enhancer etoposide was obtained from Sigma-Aldrich. The UPR inducer tunicamycin was obtained from Tocris Bioscience.

Plasmids

MERS-CoV viral mRNA was purified from infected cell lysates using the RNeasy Kit (Qiagen) and reverse-transcribed with the Transcriptor First Strand cDNA Synthesis Kit (Roche). MERS-CoV E, M, and N genes were PCR-amplified with specific primers and flanked at 5′ with Eco RI and 3′ with a 6× His tag, followed by Not I. The PCR products were digested with Eco RI and Not I, gel-purified, and cloned into the eukaryotic expression plasmid pCAGEN, resulting in pCAGEN-MERS-CoV-E-His, pCAGEN-MERS-CoV-M-His, and pCAGEN-MERS-CoV-N-His. The pCAGEN-MERS-CoV-M-His served as the template for cloning the M mutants including pCAGEN-MERS-CoV-MΔTM1, pCAGEN-MERS-CoV-MΔTM12, and pCAGEN-MERS-CoV-MΔTM123.

Transcriptome analysis

Differentially expressed cell death–associated genes were analyzed from the transcriptomic profile of MERS-CoV– and mock-infected Calu3 cells (Sequence Read Archive accession: SRP056612) (*14*). Sequencing reads were mapped to the Genome Reference Consortium GRCh37 assembly using TopHat2. Aligned BAM files were sorted by using SAMtools. GenomicAlignments and DESeq2 R packages were used for read counting and differential expression analysis. Genes with absolute value of $\log_2$ fold change greater than 1 and adjusted *P* value (Benjamini-Hochberg) less than 0.05 were considered as differentially expressed. The STRING database (version 10.5, http://string-db.org/) (*19*) was used to create a PPI network of the cell death–associated DEGs using the most direct neighboring genes of PERK at 12 hours upon MERS-CoV infection. Cytoscape (version 3.7.0, www.cytoscape.org/) was used to analyze and visualize the interactions of the PPI network.

CHOP-Luc reporter assay

Dual-luciferase reporter assay was performed with the Dual-Luciferase Reporter Assay System (Promega). Briefly, Huh7 cells were first cotransfected with the reporter plasmid pCHOP-Luc and the internal control plasmid pRL-SV40, followed by MERS-CoV infection at 1 multiplicity of infection (MOI). At 24 hpi, the infected cell lysates were harvested, and relative luciferase activity was determined by normalizing the relative luciferase unit readout of the firefly luciferase to that of the *Renilla* luciferase activity measured by the Vector X3 multilabel plate reader (PerkinElmer). Tunicamycin (1 μg/ml)–treated cells were used as a positive control.

Pseudovirus entry assay

MERS-CoV-S pseudovirus was generated using a protocol that we previously described (*48*). To evaluate the effect of PERK (GSK2656157 and AMG PERK 44) and caspase (z-VAD-fmk, z-IETD-fmk, and z-LEHD-fmk) inhibitors on MERS-CoV-S pseudovirus entry, Huh7 cells were treated with the inhibitors for 1 hour before inoculating with the MERS-CoV-S pseudoviruses. The inoculum was removed, and cells were washed at 2 hours after inoculation. At 24 hours after inoculation, the cells were lysed for detection of luciferase signal with a luciferase assay system (Promega).

Coimmunoprecipitation

Briefly, cells were lysed on ice with radioimmunoprecipitation assay coimmunoprecipitation (RIPA co-IP) buffer [50 mM tris-HCl, 150 mM NaCl, 0.1% Triton X-100, and 1% NP-40 (pH 7.4)] containing 1× protease inhibitor cocktail (Roche) and 1× phosphatase inhibitor (Thermo Fisher Scientific). The lysates were incubated with primary antibodies at room temperature for 2 hours. Protein A/G beads (Bio-Rad) were then washed with the RIPA-co-IP buffer and added into the cell lysates for overnight incubation at 4°C. After the incubation, beads were washed five times with the RIPA-co-IP buffer and eluted in 1× SDS–polyacrylamide gel electrophoresis loading

buffer by heating at 95°C for 10 min. The presence of immunoprecipitated protein in the eluent was detected with Western blots.

Quantitative reverse transcription polymerase chain reaction (RT-qPCR)

Cells were lysed in RL buffer and extracted with the MiniBEST Universal RNA Extraction Kit (TaKaRa). Viral RNA in the supernatant was extracted with the MiniBEST Viral RNA/DNA Extraction Kit (TaKaRa). RT and qPCR were performed with Transcriptor First Strand cDNA Synthesis Kit and LightCycler 480 master mix from Roche as we previously described (*49*). Primers and probes used in RT-qPCR reactions were listed in table S3. Human gene expression was normalized to human glyceraldehyde-3-phosphate dehydrogenase mRNA, whereas the mouse gene expression was normalized to mouse β-actin mRNA. Fold change in gene expression was quantified using the $\Delta\Delta C_t$ method.

Caspase and cell viability assays

The Caspase-Glo-3/7 assay (Promega) was used to quantify the activation of executor caspases including caspase-3 and caspase-7. Cells were lysed with the Caspase-Glo-3/7 reagent at the designated time points and were incubated at room temperature for 20 min, followed by measuring the luminescence signal with the Vector X3 multilabel plate reader (PerkinElmer). Cell viability was quantified with the CellTiter-Glo assay (Promega). Cells were lysed together with culture supernatant at a 1:1 ratio (volume) with the CellTiter-Glo reagent and were incubated at room temperature for 10 min, followed by measuring the luminescence signal with the Vector X3 multilabel plate reader (PerkinElmer).

siRNA knockdown

SMARTpool ON-TARGETplus human PERK siRNA and ON-TARGETplus nontargeting pool siRNA were obtained from Dharmacon. Transfection of siRNA was performed using Lipofectamine RNAiMAX (Thermo Fisher Scientific). Briefly, the cells were transfected with 70 nM siRNA for two consecutive days. At 24 hours after the second siRNA transfection, the cells were counted and harvested in RIPA buffer for Western blots. In parallel, siRNA-transfected cells were challenged with MERS-CoV at 0.1 or 1 MOI for 1 hour at 37°C. Following virus inoculation, the cells were washed with PBS and incubated in DMEM for 24 hours. At 24 hpi, the cells were lysed for Western blot analysis or for caspase-3/7 assays.

Immunofluorescence staining

After fixation for 24 hours in 10% neutral-buffered formalin, the human and mice lung tissues were processed with a TP1020 Leica semienclosed benchtop tissue processor with serially increasing concentration of ethanol, xylene, and wax for 16 hours. Processed tissues were embedded with paraffin and sectioned at 5 μm with a Thermo Fisher Scientific HM 355S rotary microtome. Tissue sections were fished and dried to fix on Thermo Fisher Scientific Superfrost Plus slides at 37°C overnight before deparaffinizing and immunofluorescence staining. Antigen retrieval was performed by heating the slides in the antigen unmasking solution (Vector Laboratories) in a pressure cooker for 90 s. MERS-CoV was detected with an in-house polyclonal guinea pig anti-N serum. Caspase-3 activation was detected with a rabbit anti–caspase-3 antibody from Abcam. For the MERS-CoV M–transfected Huh7 cells, the localization of M protein was identified with an anti-His antibody from Abcam. Rabbit anti-PDI and rabbit anti-GRP78 antibodies were obtained from Abcam. Cell nuclei were labeled with the 4′,6-diamidino-2-phenylindole (DAPI) nucleic acid stain from Thermo Fisher Scientific. Alexa Fluor secondary antibodies were obtained from Thermo Fisher Scientific. Mounting was performed with the ProLong Diamond Antifade mountant from Thermo Fisher Scientific. Images were acquired with confocal microscopy using a Zeiss LSM780 system with the 20× or the 40× oil immersion objective. Image fields were selected and processed with the ZEN software black edition (Zeiss) at the resolution of 1024 × 1024 pixels. To quantify the fluorescence intensity, representative images from multiple human or mouse lungs were split into separate channels, and the integrated intensity of channel 488 and 561 nm was quantified with ImageJ.

Histology and immunohistochemistry staining

Fixed mouse and human tissues were processed, embedded, and cut to prepare 5-μm tissue sections on glass slides. Slides were dewaxed with xylene and serially decreased concentrations of ethanol before staining. For hematoxylin and eosin (H&E) staining, tissue sections were stained with Gill's H&E Y (Thermo Fisher Scientific) as we previously described (*50*). To detect the MERS-CoV N protein, tissue sections underwent the same antigen retrieval procedures as that of immunofluorescence staining, followed by blocking with 0.3% hydrogen peroxide for 30 min to abolish the activity of any potential endogenous peroxidase. Slides were sequentially incubated with the guinea pig anti-N serum and HRP-conjugated goat anti–guinea pig antibody, followed by developing with the 3,3′-diaminobenzidine substrate kit (Vector Laboratories). The nuclei were counterstained with Gill's hematoxylin before mounting the slides with VectaMount permanent mounting medium (Vector Laboratories). Images were acquired with the Olympus BX53 light microscope using a 20× objective. To quantify the severity of the virus-induced lung damage, H&E images from multiple mouse lungs were scored as "normal/0" (absence of abnormalities), "mildly affected/1" (< 25% affected area per field), "moderately affected/2" (25 to 50% affected area per field), and "severely affected/3" (>50% affected area per field) by examining four representative pathological abnormalities commonly observed in respiratory virus infection including inflammatory infiltrations, architectural damage in the respiratory tract, proteinaceous exudates, and alveolar hemorrhage. Rating of each pathological signs of the same image was summed to generate a final score ranging from 0 (normal) to 12 (most severe) points.

Study approval

Human lung tissues for ex vivo studies were retrieved from patients who underwent surgical operations at the Queen Mary Hospital, Hong Kong. All donors gave written consent as approved by the Institutional Review Board of HKU/Hospital Authority Hong Kong West Cluster. The use of animals was approved by the Committee on the Use of Live Animals in Teaching and Research of HKU.

Statistics

Data on figures represented means and SDs. Statistical details of experiments can be found in the figure legends. Statistical comparison between different groups was performed by one-way analysis of variance (ANOVA), two-way ANOVA, Student's *t* test, or log-rank (Mantel-Cox) test using GraphPad Prism 6. Differences were considered statistically significant when $P < 0.05$. * represented $P < 0.05$,

** represented $P < 0.01$, *** represented $P < 0.001$, and **** represented $P < 0.0001$.

SUPPLEMENTARY MATERIALS

Supplementary material for this article is available at http://advances.sciencemag.org/cgi/content/full/7/25/eabf8577/DC1

View/request a protocol for this paper from *Bio-protocol*.

REFERENCES AND NOTES

1. J. S. M. Peiris, S. T. Lai, L. L. M. Poon, Y. Guan, L. Y. C. Yam, W. Lim, J. Nicholls, W. K. S. Yee, W. W. Yan, M. T. Cheung, V. C. C. Cheng, K. H. Chan, D. N. C. Tsang, R. W. H. Yung, T. K. Ng, K. Y. Yuen; SARS study group, Coronavirus as a possible cause of severe acute respiratory syndrome. *Lancet* **361**, 1319–1325 (2003).
2. A. M. Zaki, S. van Boheemen, T. M. Bestebroer, A. D. M. E. Osterhaus, R. A. M. Fouchier, Isolation of a novel coronavirus from a man with pneumonia in Saudi Arabia. *N. Engl. J. Med.* **367**, 1814–1820 (2012).
3. J. F.-W. Chan, S. Yuan, K.-H. Kok, K. K.-W. To, H. Chu, J. Yang, F. Xing, J. Liu, C. C.-Y. Yip, R. W.-S. Poon, H.-W. Tsoi, S. K.-F. Lo, K.-H. Chan, V. K.-M. Poon, W.-M. Chan, J. D. Ip, J.-P. Cai, V. C.-C. Cheng, H. Chen, C. K.-M. Hui, K.-Y. Yuen, A familial cluster of pneumonia associated with the 2019 novel coronavirus indicating person-to-person transmission: A study of a family cluster. *Lancet* **395**, 514–523 (2020).
4. N. Zhu, D. Zhang, W. Wang, X. Li, B. Yang, J. Song, X. Zhao, B. Huang, W. Shi, R. Lu, P. Niu, F. Zhan, X. Ma, D. Wang, W. Xu, G. Wu, G. F. Gao, W. Tan; China Novel Coronavirus Investigating and Research Team, A novel coronavirus from patients with pneumonia in China, 2019. *N. Engl. J. Med.* **382**, 727–733 (2020).
5. A. Roulston, R. C. Marcellus, P. E. Branton, Viruses and apoptosis. *Annu. Rev. Microbiol.* **53**, 577–628 (1999).
6. M. A. Matthay, R. L. Zemans, The acute respiratory distress syndrome: Pathogenesis and treatment. *Annu. Rev. Pathol.* **6**, 147–163 (2011).
7. T. N. Chau, K. C. Lee, H. Yao, T. Y. Tsang, T. C. Chow, Y. C. Yeung, K. W. Choi, Y. K. Tso, T. Lau, S. T. Lai, C. L. Lai, SARS-associated viral hepatitis caused by a novel coronavirus: Report of three cases. *Hepatology* **39**, 302–310 (2004).
8. Y. Ding, H. Wang, H. Shen, Z. Li, J. Geng, H. Han, J. Cai, X. Li, W. Kang, D. Weng, Y. Lu, D. Wu, L. He, K. Yao, The clinical pathology of severe acute respiratory syndrome (SARS): A report from China. *J. Pathol.* **200**, 282–289 (2003).
9. S. A. Kopecky-Bromberg, L. Martinez-Sobrido, P. Palese, 7a protein of severe acute respiratory syndrome coronavirus inhibits cellular protein synthesis and activates p38 mitogen-activated protein kinase. *J. Virol.* **80**, 785–793 (2006).
10. Y.-X. Tan, T. H. P. Tan, M. J.-R. Lee, P.-Y. Tham, V. Gunalan, J. Druce, C. Birch, M. Catton, N. Y. Fu, V. C. Yu, Y.-J. Tan, Induction of apoptosis by the severe acute respiratory syndrome coronavirus 7a protein is dependent on its interaction with the Bcl-X_L protein. *J. Virol.* **81**, 6346–6355 (2007).
11. H. Tsoi, L. Li, Z. S. Chen, K.-F. Lau, S. K. W. Tsui, H. Y. E. Chan, The SARS-coronavirus membrane protein induces apoptosis via interfering with PDK1–PKB/Akt signalling. *Biochem. J.* **464**, 439–447 (2014).
12. X. Tao, T. E. Hill, C. Morimoto, C. J. Peters, T. G. Ksiazek, C.-T. J. Tseng, Bilateral entry and release of Middle East respiratory syndrome coronavirus induces profound apoptosis of human bronchial epithelial cells. *J. Virol.* **87**, 9953–9958 (2013).
13. H. Chu, J. Zhou, B. H.-Y. Wong, C. Li, J. F.-W. Chan, Z.-S. Cheng, D. Yang, D. Wang, A. C.-Y. Lee, C. Li, M.-L. Yeung, J.-P. Cai, I. H.-Y. Chan, W.-K. Ho, K. K.-W. To, B.-J. Zheng, Y. Yao, C. Qin, K.-Y. Yuen, Middle East respiratory syndrome coronavirus efficiently infects human primary T lymphocytes and activates the extrinsic and intrinsic apoptosis pathways. *J Infect Dis* **213**, 904–914 (2016).
14. M.-L. Yeung, Y. Yao, L. Jia, J. F. W. Chan, K.-H. Chan, K.-F. Cheung, H. Chen, V. K. M. Poon, A. K. L. Tsang, K. K. W. To, M.-K. Yiu, J. L. L. Teng, H. Chu, J. Zhou, Q. Zhang, W. Deng, S. K. P. Lau, J. Y. N. Lau, P. C. Y. Woo, T.-M. Chan, S. Yung, B.-J. Zheng, D.-Y. Jin, P. W. Mathieson, C. Qin, K.-Y. Yuen, MERS coronavirus induces apoptosis in kidney and lung by upregulating Smad7 and FGF2. *Nat. Microbiol.* **1**, 16004 (2016).
15. N. Zhu, W. Wang, Z. Liu, C. Liang, W. Wang, F. Ye, B. Huang, L. Zhao, H. Wang, W. Zhou, Y. Deng, L. Mao, C. Su, G. Qiang, T. Jiang, J. Zhao, G. Wu, J. Song, W. Tan, Morphogenesis and cytopathic effect of SARS-CoV-2 infection in human airway epithelial cells. *Nat. Commun.* **11**, 3910 (2020).
16. R. Pei, J. Feng, Y. Zhang, H. Sun, L. Li, X. Yang, J. He, S. Xiao, J. Xiong, Y. Lin, K. Wen, H. Zhou, J. Chen, Z. Rong, X. Chen, Human embryonic stem cell-derived lung organoids: A model for SARS-CoV-2 infection and drug test. bioRxiv 2020.08.10.244350 [Preprint]. 10 August 2020. https://doi.org/10.1101/2020.08.10.244350.
17. J. F.-W. Chan, A. J. Zhang, S. Yuan, V. K.-M. Poon, C. C.-S. Chan, A. C.-Y. Lee, W.-M. Chan, Z. Fan, H.-W. Tsoi, L. Wen, R. Liang, J. Cao, Y. Chen, K. Tang, C. Luo, J.-P. Cai, K.-H. Kok, H. Chu, K.-H. Chan, S. Sridhar, Z. Chen, H. Chen, K. K.-W. To, K.-Y. Yuen, Simulation of the clinical and pathological manifestations of Coronavirus Disease 2019 (COVID-19) in golden Syrian hamster model: Implications for disease pathogenesis and transmissibility. *Clin. Infect. Dis.* **71**, 2428–2446 (2020).
18. S. Li, L. Jiang, X. Li, F. Lin, Y. Wang, B. Li, T. Jiang, W. An, S. Liu, H. Liu, P. Xu, L. Zhao, L. Zhang, J. Mu, H. Wang, J. Kang, Y. Li, L. Huang, C. Zhu, S. Zhao, J. Lu, J. Ji, J. Zhao, Clinical and pathological investigation of patients with severe COVID-19. *JCI Insight* **5**, e138070 (2020).
19. D. Szklarczyk, J. H. Morris, H. Cook, M. Kuhn, S. Wyder, M. Simonovic, A. Santos, N. T. Doncheva, A. Roth, P. Bork, L. J. Jensen, C. von Mering, The STRING database in 2017: Quality-controlled protein-protein association networks, made broadly accessible. *Nucleic Acids Res.* **45**, D362–D368 (2017).
20. J. Han, S. H. Back, J. Hur, Y. H. Lin, R. Gildersleeve, J. Shan, C. L. Yuan, D. Krokowski, S. Wang, M. Hatzoglou, M. S. Kilberg, M. A. Sartor, R. J. Kaufman, ER-stress-induced transcriptional regulation increases protein synthesis leading to cell death. *Nat. Cell Biol.* **15**, 481–490 (2013).
21. C. Hetz, F. R. Papa, The unfolded protein response and cell fate control. *Mol. Cell* **69**, 169–181 (2018).
22. Z. Liu, Y. Lv, N. Zhao, G. Guan, J. Wang, Protein kinase R-like ER kinase and its role in endoplasmic reticulum stress-decided cell fate. *Cell Death Dis.* **6**, e1822 (2015).
23. P. Pihan, A. Carreras-Sureda, C. Hetz, BCL-2 family: Integrating stress responses at the ER to control cell demise. *Cell Death Differ.* **24**, 1478–1487 (2017).
24. J. Kale, E. J. Osterlund, D. W. Andrews, BCL-2 family proteins: Changing partners in the dance towards death. *Cell Death Differ.* **25**, 65–80 (2018).
25. P. F. Connolly, H. O. Fearnhead, Viral hijacking of host caspases: An emerging category of pathogen-host interactions. *Cell Death Differ.* **24**, 1401–1410 (2017).
26. A. Richard, D. Tulasne, Caspase cleavage of viral proteins, another way for viruses to make the best of apoptosis. *Cell Death Dis.* **3**, e277 (2012).
27. D. L. Ng, F. Al Hosani, M. K. Keating, S. I. Gerber, T. L. Jones, M. G. Metcalfe, S. Tong, Y. Tao, N. N. Alami, L. M. Haynes, M. A. Mutei, L. Abdel-Wareth, T. M. Uyeki, D. L. Swerdlow, M. Barakat, S. R. Zaki, Clinicopathologic, immunohistochemical, and ultrastructural findings of a fatal case of Middle East respiratory syndrome coronavirus infection in the United Arab Emirates, April 2014. *Am. J. Pathol.* **186**, 652–658 (2016).
28. A. C. Hocke, A. Becher, J. Knepper, A. Peter, G. Holland, M. Tonnies, T. T. Bauer, P. Schneider, J. Neudecker, D. Muth, C. M. Wendtner, J. C. Ruckert, C. Drosten, A. D. Gruber, M. Laue, N. Suttorp, S. Hippenstiel, T. Wolff, Emerging human middle East respiratory syndrome coronavirus causes widespread infection and alveolar damage in human lungs. *Am. J. Respir. Crit. Care Med.* **188**, 882–886 (2013).
29. P. Venkatagopalan, S. M. Daskalova, L. A. Lopez, K. A. Dolezal, B. G. Hogue, Coronavirus envelope (E) protein remains at the site of assembly. *Virology* **478**, 75–85 (2015).
30. H. Vennema, G. J. Godeke, J. W. Rossen, W. F. Voorhout, M. C. Horzinek, D. J. Opstelten, P. J. Rottier, Nucleocapsid-independent assembly of coronavirus-like particles by co-expression of viral envelope protein genes. *EMBO J.* **15**, 2020–2028 (1996).
31. A. Bertolotti, Y. Zhang, L. M. Hendershot, H. P. Harding, D. Ron, Dynamic interaction of BiP and ER stress transducers in the unfolded-protein response. *Nat. Cell Biol.* **2**, 326–332 (2000).
32. Y. L. Siu, K. T. Teoh, J. Lo, C. M. Chan, F. Kien, N. Escriou, S. W. Tsao, J. M. Nicholls, R. Altmeyer, J. S. M. Peiris, R. Bruzzone, B. Nal, The M, E, and N structural proteins of the severe acute respiratory syndrome coronavirus are required for efficient assembly, trafficking, and release of virus-like particles. *J. Virol.* **82**, 11318–11330 (2008).
33. C. A. de Haan, L. Kuo, P. S. Masters, H. Vennema, P. J. Rottier, Coronavirus particle assembly: Primary structure requirements of the membrane protein. *J. Virol.* **72**, 6838–6850 (1998).
34. J. K. Locker, J. K. Rose, M. C. Horzinek, P. J. Rottier, Membrane assembly of the triple-spanning coronavirus M protein. Individual transmembrane domains show preferred orientation. *J. Biol. Chem.* **267**, 21911–21918 (1992).
35. S. Herold, M. Steinmueller, W. von Wulffen, L. Cakarova, R. Pinto, S. Pleschka, M. Mack, W. A. Kuziel, N. Corazza, T. Brunner, W. Seeger, J. Lohmeyer, Lung epithelial apoptosis in influenza virus pneumonia: The role of macrophage-expressed TNF-related apoptosis-inducing ligand. *J. Exp. Med.* **205**, 3065–3077 (2008).
36. R. Brauer, L. Ge, S. Y. Schlesinger, T. P. Birkland, Y. Huang, T. Parimon, V. Lee, B. L. McKinney, J. K. McGuire, W. C. Parks, P. Chen, Syndecan-1 attenuates lung injury during influenza infection by potentiating c-Met signaling to suppress epithelial apoptosis. *Am. J. Respir. Crit. Care Med.* **194**, 333–344 (2016).
37. Y. Liao, T. S. Fung, M. Huang, S. G. Fang, Y. Zhong, D. X. Liu, Upregulation of CHOP/GADD153 during coronavirus infectious bronchitis virus infection modulates apoptosis by restricting activation of the extracellular signal-regulated kinase pathway. *J. Virol.* **87**, 8124–8134 (2013).
38. Y. Ren, T. Shu, D. Wu, J. Mu, C. Wang, M. Huang, Y. Han, X. Y. Zhang, W. Zhou, Y. Qiu, X. Zhou, The ORF3a protein of SARS-CoV-2 induces apoptosis in cells. *Cell. Mol. Immunol.* **17**, 881–883 (2020).
39. K.-L. Siu, K.-H. Kok, M.-H. Ng, V. K. M. Poon, K.-Y. Yuen, B.-J. Zheng, D.-Y. Jin, Severe acute respiratory syndrome coronavirus M protein inhibits type I interferon production by

impeding the formation of TRAF3·TANK·TBK1/IKKε complex. *J. Biol. Chem.* **284**, 16202–16209 (2009).
40. P.-Y. Lui, L.-Y. Wong, C.-L. Fung, K.-L. Siu, M.-L. Yeung, K.-S. Yuen, C.-P. Chan, P. C.-Y. Woo, K.-Y. Yuen, D.-Y. Jin, Middle East respiratory syndrome coronavirus M protein suppresses type I interferon expression through the inhibition of TBK1-dependent phosphorylation of IRF3. *Emerg. Microbes Infect.* **5**, e39 (2016).
41. C. A. Benedict, P. S. Norris, C. F. Ware, To kill or be killed: Viral evasion of apoptosis. *Nat. Immunol.* **3**, 1013–1018 (2002).
42. W. J. Wurzer, O. Planz, C. Ehrhardt, M. Giner, T. Silberzahn, S. Pleschka, S. Ludwig, Caspase 3 activation is essential for efficient influenza virus propagation. *EMBO J.* **22**, 2717–2728 (2003).
43. H. Chu, J. F.-W. Chan, T. T.-T. Yuen, H. Shuai, S. Yuan, Y. Wang, B. Hu, C. C.-Y. Yip, J. O.-L. Tsang, X. Huang, Y. Chai, D. Yang, Y. Hou, K. K.-H. Chik, X. Zhang, A. Y.-F. Fung, H.-W. Tsoi, J.-P. Cai, W.-M. Chan, J. D. Ip, A. W.-H. Chu, J. Zhou, D. C. Lung, K.-H. Kok, K. K.-W. To, O. T.-Y. Tsang, K.-H. Chan, K.-Y. Yuen, Comparative tropism, replication kinetics, and cell damage profiling of SARS-CoV-2 and SARS-CoV with implications for clinical manifestations, transmissibility, and laboratory studies of COVID-19: An observational study. *Lancet Microbe* **1**, e14–e23 (2020).
44. H. Chu, J. F.-W. Chan, Y. Wang, T. T.-T. Yuen, Y. Chai, Y. Hou, H. Shuai, D. Yang, B. Hu, X. Huang, X. Zhang, J.-P. Cai, J. Zhou, S. Yuan, K.-H. Kok, K. K.-W. To, I. H.-Y. Chan, A. J. Zhang, K.-Y. Sit, W.-K. Au, K.-Y. Yuen, Comparative replication and immune activation profiles of SARS-CoV-2 and SARS-CoV in human lungs: An ex vivo study with implications for the pathogenesis of COVID-19. *Clin. Infect. Dis.* **71**, 1400–1409 (2020).
45. J. Zhou, C. Li, G. Zhao, H. Chu, D. Wang, H. H.-N. Yan, K.-M. Poon, L. Wen, B. H.-Y. Wong, X. Zhao, M. C. Chiu, D. Yang, Y. Wang, R. K. H. Au-Yeung, I. H.-Y. Chan, S. Sun, J. F.-W. Chan, K. K.-W. To, Z. A. Memish, V. M. Corman, C. Drosten, I. F.-N. Hung, Y. Zhou, S. Y. Leung, K.-Y. Yuen, Human intestinal tract serves as an alternative infection route for Middle East respiratory syndrome coronavirus. *Sci. Adv.* **3**, eaao4966 (2017).
46. K. Li, C. L. Wohlford-Lenane, R. Channappanavar, J.-E. Park, J. T. Earnest, T. B. Bair, A. M. Bates, K. A. Brogden, H. A. Flaherty, T. Gallagher, D. K. Meyerholz, S. Perlman, P. B. McCray Jr., Mouse-adapted MERS coronavirus causes lethal lung disease in human DPP4 knockin mice. *Proc. Natl. Acad. Sci. U.S.A.* **114**, E3119–E3128 (2017).
47. P. B. McCray Jr., L. Pewe, C. Wohlford-Lenane, M. Hickey, L. Manzel, L. Shi, J. Netland, H. P. Jia, C. Halabi, C. D. Sigmund, D. K. Meyerholz, P. Kirby, D. C. Look, S. Perlman, Lethal infection of K18-*hACE2* mice infected with severe acute respiratory syndrome coronavirus. *J. Virol.* **81**, 813–821 (2007).
48. H. Chu, B. Hu, X. Huang, Y. Chai, D. Zhou, Y. Wang, H. Shuai, D. Yang, Y. Hou, X. Zhang, T. T.-T. Yuen, J.-P. Cai, A. J. Zhang, J. Zhou, S. Yuan, K. K.-W. To, I. H.-Y. Chan, K.-Y. Sit, D. C.-C. Foo, I. Y.-H. Wong, A. T.-L. Ng, T. T. Cheung, S. Y.-K. Law, W.-K. Au, M. A. Brindley, Z. Chen, K.-H. Kok, J. F.-W. Chan, K.-Y. Yuen, Host and viral determinants for efficient SARS-CoV-2 infection of the human lung. *Nat. Commun.* **12**, 134 (2021).
49. H. Shuai, H. Chu, Y. Hou, D. Yang, Y. Wang, B. Hu, X. Huang, X. Zhang, Y. Chai, J.-P. Cai, J. F.-W. Chan, K.-Y. Yuen, Differential immune activation profile of SARS-CoV-2 and SARS-CoV infection in human lung and intestinal cells: Implications for treatment with IFN-β and IFN inducer. *J. Infect.* **81**, e1–e10 (2020).
50. H. Chu, J. F.-W. Chan, Y. Wang, T. T.-T. Yuen, Y. Chai, H. Shuai, D. Yang, B. Hu, X. Huang, X. Zhang, Y. Hou, J.-P. Cai, A. J. Zhang, J. Zhou, S. Yuan, K. K.-W. To, I. F.-N. Hung, T. T. Cheung, A. T.-L. Ng, I. H.-Y. Chan, I. Y.-H. Wong, S. Y.-K. Law, D. C.-C. Foo, W. K. Leung, K. Y. Yuen, SARS-CoV-2 induces a more robust innate immune response and replicates less efficiently than SARS-CoV in the human intestines: An ex vivo study with implications on pathogenesis of COVID-19. *Cell. Mol. Gastroenterol. Hepatol.* **11**, 771–781 (2020).

Acknowledgments: We thank Ivy Hau-Yee Chan, Department of Surgery, HKU for facilitating the study. **Funding:** This work was partly supported by the donations of Michael Seak-Kan Tong, the Shaw Foundation Hong Kong, Richard Yu and Carol Yu, May Tam Mak Mei Yin, Respiratory Viral Research Foundation Limited, Lee Wan Keung Charity Foundation Limited, Hong Kong Sanatorium & Hospital, Hui Ming, Hui Hoy and Chow Sin Lan Charity Fund Limited, the Chan Yin Chuen Memorial Charitable Foundation, Marina Man-Wai Lee, the Hong Kong Hainan Commercial Association South China Microbiology Research Fund, the Jessie & George Ho Charitable Foundation, Perfect Shape Medical Limited, Kai Chong Tong, Tse Kam Ming Laurence, Foo Oi Foundation Limited, Betty Hing-Chu Lee, Ping Cham So, and the Lo Ying Shek Chi Wai Foundation. This work was also partly supported by funding from the Hong Kong Health and Medical Research Fund (16150572 and CID-HKU1-5) of the Food and Health Bureau, Hong Kong Special Administrative Region Government; the General Research Fund (17124415 and 17124220) of Research Grants Council, Hong Kong Special Administrative Region Government; Innovation and Technology Fund (ITF), the Government of the Hong Kong Special Administrative Region; the Consultancy Service for Enhancing Laboratory Surveillance of Emerging Infectious Diseases and Research Capability on Antimicrobial Resistance for Department of Health of the Hong Kong Special Administrative Region Government; the National Program on Key Research Project of China (grant no. 2020YFA0707500 and 2020YFA0707504); the HKU Seed Fund (201711159220 and 201811159126); Sanming Project of Medicine in Shenzhen, China (SZSM201911014); and the High Level-Hospital Program, Health Commission of Guangdong Province, China. **Author contributions:** Conceived and designed the experiments: H.C., H.S., J.F.-W.C., and K.-Y.Y. Performed experiments: H.C., H.S., Y.H., X. Zhang, L.W., X.H., B.H., D.Y., Y.W., C.Y., B.H.-Y.W., C.L., X. Zhao, V.K.-M.P., J.-P.C., and S.Y. Data analysis: H.C., H.S., K.K.-Y.W., M.-L.Y., J.Z., R.K.-H.A.-Y., D.-Y.J., K.-H.K., S.P., J.F.-W.C., and K.-Y.Y. Wrote the manuscript: H.C., H.S., S.P., J.F.-W.C., and K.-Y.Y. **Competing interests:** J.F.-W.C. has received travel grants from Pfizer Corporation Hong Kong and Astellas Pharma Hong Kong Corporation Limited and was an invited speaker for Gilead Sciences Hong Kong Limited and Luminex Corporation. The other authors declared no other competing interests. The funding sources had no role in study design, data collection, analysis or interpretation, or writing of the report. **Data and materials availability:** All data needed to evaluate the conclusions in the paper are present in the paper and/or the Supplementary Materials. Additional data related to this paper may be requested from the authors.

Submitted 24 November 2020
Accepted 4 May 2021
Published 16 June 2021
10.1126/sciadv.abf8577

Citation: H. Chu, H. Shuai, Y. Hou, X. Zhang, L. Wen, X. Huang, B. Hu, D. Yang, Y. Wang, C. Yoon, B. H.-Y. Wong, C. Li, X. Zhao, V. K.-M. Poon, J.-P. Cai, K. K.-Y. Wong, M.-L. Yeung, J. Zhou, R. K.-H. Au-Yeung, S. Yuan, D.-Y. Jin, K.-H. Kok, S. Perlman, J. F.-W. Chan, K.-Y. Yuen, Targeting highly pathogenic coronavirus-induced apoptosis reduces viral pathogenesis and disease severity. *Sci. Adv.* **7**, eabf8577 (2021).